A constrained maximum-SINR NBI-resistant receiver for OFDM systems

Donatella Darsena *Member, IEEE,* Giacinto Gelli, Luigi Paura, and Francesco Verde

***Abstract*— In this paper, with reference to the problem of joint equalization and narrowband interference (NBI) suppression in orthogonal frequency-division multiplexing (OFDM) systems, synthesis and analysis of both unconstrained and constrained optimum equalizers are carried out, based on the maximum signal-to-noise-plus-interference (SINR) criterion. Specifically, a comparative performance analysis is provided from a theoretical point of view, either when the second-order statistics (SOS) of the received data are exactly known at the receiver, or when they are estimated from a finite number of data samples. Relying on the results of this analysis, a three-stage constrained maximum-SINR equalizer is then proposed, which outperforms existing receivers and, in comparison with its unconstrained counterpart, exhibits a significantly stronger robustness against errors in the estimated SOS. Moreover, a computationally-efficient adaptive implementation of the three-stage equalizer is derived and, in connection with it, a simple and effective NBI-resistant channel estimation algorithm is proposed. Finally, numerical simulations are performed aimed at validating the theoretical analysis carried out and comparing the performances of the considered equalizers with those of existing approaches.**

***Index Terms*— Narrowband interference (NBI) suppression, constrained maximum signal-to-interference-plus-noise ratio (SINR) optimizations, orthogonal frequency-division multiplexing (OFDM) systems.**

I. INTRODUCTION

In many applications, such as high-speed Internet access, wireless networking, digital audio and video broadcasting, the increasing need to integrate heterogeneous services has led to very high data-rate transmission requirements, thereby making intersymbol interference (ISI), induced by channel dispersion, one of the main performance limiting factor. To counteract ISI, several physical layer solutions employ multicarrier schemes [1], [2], such as discrete multitone (DMT), orthogonal frequency-division multiplexing (OFDM), and multicarrier code-division multiple-access (MC-CDMA). OFDM schemes cope with ISI by inserting a *cyclic prefix* (CP) of length $L_{\rm cp}$ at the beginning of each transmitted symbol, which is discarded at the receiver, allowing thus the use of inexpensive detection schemes, based on Fast Fourier Transform (FFT) followed by one-tap frequency equalization (FEQ). Moreover, a suitable number $M_{\rm vc}$ of *virtual carriers* (VCs) are usually inserted into the OFDM signal [1], aimed at simplifying the design of transmitting and receiving filters.

In many scenarios, multicarrier systems operate in the presence of severe narrowband interference (NBI), e.g., in wireless systems operating in overlay mode or in non-licensed band, or in wireline ones, wherein the transmission cables might be exposed to crosstalk or radio-frequency interference. The simple FFT-based receiver exhibits very poor performances in the presence of NBI, since it merely nullifies *interblock interference* (IBI) and *interchannel interference* (ICI), without taking any specific measure to counteract noise and NBI effects, i.e., it acts as the simplest form of data-independent zero-forcing (ZF) receiver. A viable strategy to jointly counteract channel impairments and NBI in wireline DMT systems is the adoption of bit-loading techniques [3] at the transmitter, whose use, however, is problematic in wireless systems, due to the rapid changes in channel characteristics. Therefore, a preferred solution for OFDM-based wireless systems is to devise simple interference suppression algorithms at the receiver side. To perform this task, one might exploit different types of redundancy, which are present in the OFDM signals, such as the *temporal redundancy* induced by CP insertion, or the *frequency redundancy* associated with the presence of VCs.[1]

Several reception strategies targeted at *pure CP-based systems* (i.e., $M_{\rm vc} = 0$) exploit temporal redundancy, by processing the portion (so-called *unconsumed*) of the CP not contaminated by the channel, provided that the CP length $L_{\rm cp}$ exceeds the discrete-time channel order L_h. The resulting *windowing receivers* [5], [6] build (with different *ad hoc* criteria) a data-dependent window to be used before the FFT, aimed at reducing noise and NBI contributions without modifying the desired signal component. In particular, [5], [6] carry out window designs based on the minimum mean-square error (MMSE) criterion; however, the design constraints (mainly aimed at reducing receiver complexity) do not allow one to fully exploit the temporal redundancy contained in the CP, leading thus to equalizers with limited NBI suppression capabilities. For the same pure CP-based systems, an MMSE equalizer has been proposed [7], which achieves a stronger robustness against NBI effects by processing *all* the CP samples. On the other hand, when the channel order L_h is

Manuscript received ....; revised .....and....

This work is partially supported by Italian National project Wireless 8O2.16 Multi-antenna mEsh Networks (WOMEN) under grant number 2005093248.

D. Darsena is with Dipartimento per le Tecnologie, Università Parthenope, Via Medina 40, I-80133, Napoli, Italy (e-mail: darsena@unina.it). G. Gelli, L. Paura, and F. Verde are with Dipartimento di Ingegneria Elettronica e delle Telecomunicazioni, Università Federico II, via Claudio 21, I-80125, Napoli, Italy [e-mail: (gelli, paura, f.verde)@unina.it].

Publisher Item Identifier S 0000-0000(00)00000-3.

[1] As a matter of fact, besides temporal and frequency redundancy, also "constellation redundancy" [4] can be exploited to improve NBI rejection, taking advantage of symmetry properties exhibited by many constellations in digital communications.

very high, in order to avoid the large overhead arising from the insertion of a long CP, a common solution is to employ a time-domain equalizer (TEQ) before the FFT, aimed at shortening the channel impulse response. In the DMT context, relying on the idea that the TEQ and the demodulating FFT can be interchanged, the authors in [8] proposed a frequency-domain filter, so-called *per-tone equalizer* (PTEQ), that outperforms classical TEQs at the expense of a higher memory cost, by separately designing a linear MMSE equalizer for each subcarrier. It has been shown in [9] that the combination of windowing and per-tone equalization leads to the synthesis of a windowing PTEQ (WPTEQ) receiver, which exhibits increased robustness against NBI, compared to a TEQ-based receiver. Recently, the results of [8] and [9] have been extended in [10] to account for infinite impulse response (IIR) channel models.

Instead of (or in addition to) the temporal redundancy contained in the CP, one can exploit frequency redundancy arising from VC insertion to synthesize NBI-resistant receivers. The use of frequency redundancy for the synthesis of ZF generalized FEQ-DMT equalizers (operating in the absence of NBI) has been already proposed in [11], [12], [13], [14]. More precisely, receivers targeted at *pure VC-based system* (i.e., with $L_{\text{cp}} = 0$ and $M_{\text{vc}} \neq 0$) were considered in [11], whereas ZF design techniques for an hybrid CP/VC-based system (i.e., with $L_{\text{cp}} \neq 0$ and $M_{\text{vc}} \neq 0$) were proposed in [12], [13], [14]. However, all these ZF receivers lack of any NBI suppression capability. With reference to a pure VC-based system, in [15] it is also proposed an MMSE version of the FEQ-DMT receiver [11], which might also be used to counteract the NBI (even though this feature was not explicitly mentioned in [15]). A different MMSE approach to NBI rejection, which can be applied to hybrid CP/VC-based systems with $L_{\text{cp}} \geq L_h$, is proposed in [16]; it is based on a linear interference canceler that estimates, in the MMSE sense, the NBI at the receiving side, and subtract it from the received signal. The receiver of [16] is synthesized under the assumptions that the VCs are located in the frequency domain close to the NBI spectral position, and the second order statistics (SOS) of the NBI are known at the receiver; if any or both assumptions are not exactly satisfied, its performance may degrade significantly. Moreover, the same receiver can also operate in a system without VCs, but in this case it undergoes [16] a significant performance degradation. Recently, an NBI-resistant receiver has been proposed in [17], whose synthesis is based on the minimum mean-output-energy (MMOE) criterion [18]. In comparison with windowing receivers (e.g., [6]), the approach of [17] leads to a better exploitation of the temporal redundancy; however, the resulting receiver is targeted at pure CP-based systems and, hence, does not exploit the redundancy induced by VC insertion.

From the previous discussion, it appears that the NBI suppression techniques proposed in [5], [6], [8], [9], [16], [17] do not fully exploit the temporal and/or frequency redundancy of the OFDM signal. Furthermore, in many of these papers, the performance studies carried out, either theoretically or experimentally, have been based on the idealized assumption that the SOS of the received data are exactly known at the receiver. In practice, SOS must be estimated from a finite number of samples of the received signal, and the resulting data-estimated receivers can suffer from a significant performance degradation with respect to their ideal counterparts. Another limitation of all the aforementioned techniques is that the desired channel impulse response is assumed to be exactly known at the receiver; however, in the presence of strong NBI, channel estimation is quite a challenging task and cannot be performed by resorting to standard algorithms [19]. In this paper, we tackle the NBI suppression problem by casting it in a more general framework and addressing explicitly the channel estimation problem in the presence of NBI. First, we consider in Section II a general OFDM signal model, accounting for (possibly combined) insertion of CP and VCs, and encompassing, as particular cases, pure CP-based systems, pure VC-based systems and hybrid CP/VC-based systems. Relying on the maximum signal-to-interference-plus-noise ratio (SINR) criterion, we synthesize in Section III interference-resistant IBI-free receivers, which do not make use of the conventional FFT-based preprocessing, and we analyze their disturbance rejection capabilities, both when the SOS of the received data are ideally known at the receiver, as well as when the equalizers are synthesized starting from SOS estimates. In particular, we analytically show that, although the maximum-SINR equalizer is capable of ideally achieving satisfactory ICI-plus-NBI suppression under certain conditions, it suffers from a significant performance degradation when is estimated from data. Capitalizing on the results of our analysis, we design in Section IV a three-stage *constrained* maximum-SINR equalizer, which generalizes our previous formulation [17] and offers improved robustness against finite sample-size effects. For such a receiver, a theoretical performance analysis is provided, in both cases of known and estimated SOS. Moreover, a low-complexity adaptive implementation of the proposed equalizer is devised, which allows one to estimate the desired channel impulse response, even in the presence of strong NBI. Section V provides numerical results, aimed at corroborating the results of the theoretical analysis and assessing the performances of both unconstrained and constrained maximum-SINR equalizers, in different operative scenarios and in comparison with existing receivers. Finally, concluding remarks are drawn in Section VI.

A. Notations

The fields of complex, real, and integer numbers are denoted with $\mathbb{C}$, $\mathbb{R}$, and $\mathbb{Z}$, respectively; matrices [vectors] are denoted with upper [lower] case boldface letters (e.g., $\mathbf{A}$ or $\mathbf{a}$); the field of $m \times n$ complex [real] matrices is denoted as $\mathbb{C}^{m\times n}$ [$\mathbb{R}^{m\times n}$], with $\mathbb{C}^m$ [$\mathbb{R}^m$] used as a shorthand for $\mathbb{C}^{m\times 1}$ [$\mathbb{R}^{m\times 1}$]; $\{\mathbf{A}\}_{ij}$ or $\mathbf{A}_{ij}$ indicates the $(i+1, j+1)$th element of matrix $\mathbf{A} \in \mathbb{C}^{m\times n}$, with $i \in \{0, 1, \ldots, m-1\}$ and $j \in \{0, 1, \ldots, n-1\}$; the superscripts $*$, T, H, -1 and $\dagger$ denote the conjugate, the transpose, the Hermitian (conjugate transpose), the inverse, and the Moore-Penrose generalized inverse [20] (pseudo-inverse) of a matrix, respectively; $\odot$ denotes Hadamard (elementwise) product of two matrices and $\|\mathbf{a}\|$ is the Euclidean norm of $\mathbf{a}$; $\mathbf{0}_m \in \mathbb{R}^m$,

$\mathbf{O}_{m\times n} \in \mathbb{R}^{m\times n}$ and $\mathbf{I}_m \in \mathbb{R}^{m\times m}$ denote the null vector, the null matrix, and the identity matrix, respectively; $\mathcal{N}(\mathbf{A})$, $\mathcal{R}(\mathbf{A})$, and $\mathcal{R}^{\perp}(\mathbf{A})$ denote the null space, the range (column space), and the orthogonal complement of the column space of $\mathbf{A} \in \mathbb{C}^{m\times n}[\mathbb{R}^{m\times n}]$ in $\mathbb{C}^m[\mathbb{R}^m]$; when applied to a vector $\mathbf{A} = \mathrm{diag}(\mathbf{a})$ is the diagonal matrix with $\mathbf{A}_{ii} = \mathbf{a}_i$, whereas when applied to a matrix $\mathbf{a} = \mathrm{diag}(\mathbf{A})$ is the vector with $\mathbf{a}_i = \mathbf{A}_{ii}$; finally, $\mathrm{E}[\cdot]$, $\star$ and $\lceil\cdot\rceil$ denote ensemble averaging, convolution and integer ceiling, respectively.

II. OFDM SYSTEM MODEL AND MAXIMUM-SINR OPTIMIZATION

Let us consider an hybrid CP/VC-based OFDM system with M subcarriers, Q of which are utilized, whereas the remaining $M_{\mathrm{vc}} \triangleq M - Q$ are VCs. At the transmitter, the information data stream $s(n)$ ($n \in \mathbb{Z}$) is converted into Q parallel substreams $s_q(n) \triangleq s(nQ+q)$, where $q \in \{0,1,\ldots,Q-1\}$ refers to the subcarrier. By assuming for now that the VCs are inserted at the end of the nth data block $\mathbf{s}(n) \triangleq [s_0(n), s_1(n), \ldots, s_{Q-1}(n)]^T \in \mathbb{C}^Q$, one obtains, after VC insertion, the new symbol block $\widetilde{\mathbf{s}}(n) \triangleq [\widetilde{s}_0(n), \widetilde{s}_1(n), \ldots, \widetilde{s}_{M-1}(n)]^T \in \mathbb{C}^M$, which can be expressed as $\widetilde{\mathbf{s}}(n) = \mathbf{S}\,\mathbf{s}(n)$, where $\mathbf{S} \triangleq [\mathbf{I}_Q, \mathbf{O}^T_{M_{\mathrm{vc}}\times Q}]^T \in \mathbb{R}^{M\times Q}$ is tall and full-column rank. This relation can be generalized to allow for VCs insertion[2] in arbitrary positions $\mathcal{I}_{\mathrm{vc}} = \{q_0, q_1, \ldots, q_{M_{\mathrm{vc}}-1}\}$, by introducing a row-permutation matrix [21] $\mathbf{P} \in \mathbb{R}^{M\times M}$, i.e., $\widetilde{\mathbf{s}}(n) = \mathbf{\Theta}\,\mathbf{s}(n)$, with $\mathbf{\Theta} \triangleq \mathbf{P}\,\mathbf{S} \in \mathbb{R}^{M\times Q}$. Subsequently, the block $\widetilde{\mathbf{s}}(n)$ is subject to the Inverse Discrete Fourier Transform (IDFT), obtaining the vector $\widetilde{\mathbf{u}}(n) = \mathbf{W}_{\mathrm{IDFT}}\,\mathbf{\Theta}\,\mathbf{s}(n) \in \mathbb{C}^M$, where $\{\mathbf{W}_{\mathrm{IDFT}}\}_{mp} \triangleq (1/\sqrt{M})\, e^{j\frac{2\pi}{M}mp}$, with $m,p \in \{0,1,\ldots,M-1\}$, represents the unitary symmetric IDFT matrix[3]. Then, a CP of length L_{cp} is inserted at the beginning of $\widetilde{\mathbf{u}}(n)$, thus obtaining $\mathbf{u}(n) \triangleq [u_0(n), u_1(n), \ldots, u_{P-1}(n)]^T \in \mathbb{C}^P$, with $P \triangleq M + L_{\mathrm{cp}}$, which can be expressed as $\mathbf{u}(n) \triangleq \mathbf{T}_0\,\mathbf{s}(n)$, where $\mathbf{T}_0 \triangleq \mathbf{T}_{\mathrm{cp}}\,\mathbf{W}_{\mathrm{IDFT}}\,\mathbf{\Theta} \in \mathbb{C}^{P\times Q}$ is the full-column rank *precoding* matrix, with $\mathbf{T}_{\mathrm{cp}} \triangleq [\mathbf{I}^T_{\mathrm{cp}}, \mathbf{I}_M]^T \in \mathbb{R}^{P\times M}$ and $\mathbf{I}_{\mathrm{cp}} \in \mathbb{R}^{L_{\mathrm{cp}}\times M}$ is obtained from $\mathbf{I}_M$ by picking its last L_{cp} rows. Vector $\mathbf{u}(n)$ undergoes parallel-to-serial conversion, and the resulting sequence $\{u_p(n)\}_{p=0}^{P-1}$ feeds a digital-to-analog converter (DAC), operating at rate $1/T_c = P/T$, where T_c and T denote the sampling and the symbol period, respectively. After up-conversion, the continuous-time signal $u_c(t)$ at the DAC output is transmitted over a multipath channel, which is modeled as a linear time-invariant (LTI) system with impulse response $g_c(t)$.

After antialiasing filtering, the received baseband signal is given by $\widetilde{r}_c(t) = u_c(t) \star g_c(t) \star \phi_c(t) + \widetilde{\jmath}_c(t) + \widetilde{w}_c(t)$, where $\phi_c(t)$ is the impulse response of the analog-to-digital (ADC) antialiasing filter, whereas $\widetilde{\jmath}_c(t)$ and $\widetilde{w}_c(t)$ account for the interference and thermal noise at the output of the ADC filter. Denote with $h_c(t)$ the impulse response of the *composite* channel (encompassing the cascade of the DAC filter, the physical channel, and the ADC filter), which spans $L_h < P$ sampling periods, that is, $h_c(t) \equiv 0$ for $t \notin [0, L_h\,T_c]$. After ideal carrier-frequency recovery, sampling with rate $1/T_c$ and removing only L_h samples of the CP to achieve perfect IBI suppression, the nth ($n \in \mathbb{Z}$) IBI-free received data block $\mathbf{r}(n) \in \mathbb{C}^N$, with $N \triangleq P - L_h > 0$, can be expressed (see [2], [22]) as

$$\mathbf{r}(n) \triangleq \mathbf{R}_{L_h}\widetilde{\mathbf{r}}(n) = \underbrace{\mathbf{H}\,\mathbf{T}_0}_{\mathbf{F}_0\in\mathbb{C}^{N\times Q}}\,\mathbf{s}(n) + \boldsymbol{\jmath}(n) + \mathbf{w}(n) = \mathbf{F}_0\,\mathbf{s}(n) + \boldsymbol{\jmath}(n) + \mathbf{w}(n)\,, \quad (1)$$

where the matrix $\mathbf{R}_{L_h} \triangleq [\mathbf{O}_{N\times L_h}, \mathbf{I}_N] \in \mathbb{R}^{N\times P}$ discards the first L_h entries of the received vector $\widetilde{\mathbf{r}}(n) \triangleq [\widetilde{r}_0(n), \widetilde{r}_1(n), \ldots, \widetilde{r}_{P-1}(n)]^T \in \mathbb{C}^P$, which collects all the samples $\widetilde{r}_\ell(n) \triangleq \widetilde{r}_c(n\,T + \ell\,T_c)$; whereas $\mathbf{H} \in \mathbb{C}^{N\times P}$ is the Toeplitz channel matrix, whose first column and row are given by $[h(L_h), 0, \ldots, 0]^T$ and $[h(L_h), \ldots, h(0), 0, \ldots, 0]$, respectively, depending on the discrete time channel $h(m) \triangleq h_c(mT_c)$, which is a causal finite impulse response (FIR) filter of order L_h, i.e., $h(m) \equiv 0$ for $m \notin \{0,1,\ldots,L_h\}$, with $h(0), h(L_h) \neq 0$; and, finally, $\boldsymbol{\jmath}(n) \triangleq \mathbf{R}_{L_h}\widetilde{\boldsymbol{\jmath}}(n) \in \mathbb{C}^N$ and $\mathbf{w}(n) \triangleq \mathbf{R}_{L_h}\widetilde{\mathbf{w}}(n) \in \mathbb{C}^N$ represent the NBI and the noise vectors, respectively, where $\widetilde{\boldsymbol{\jmath}}(n) \triangleq [\widetilde{\jmath}_0(n), \widetilde{\jmath}_1(n), \ldots, \widetilde{\jmath}_{P-1}(n)]^T \in \mathbb{C}^P$ and $\widetilde{\mathbf{w}}(n) \triangleq [\widetilde{w}_0(n), \widetilde{w}_1(n), \ldots, \widetilde{w}_{P-1}(n)]^T \in \mathbb{C}^P$, with $\widetilde{\jmath}_\ell(n) \triangleq \widetilde{\jmath}_c(n\,T + \ell\,T_c)$ and $\widetilde{w}_\ell(n) \triangleq \widetilde{w}_c(n\,T + \ell\,T_c)$. It is worth noting that, unlike many equalization techniques for *pure CP-based systems* (i.e., $M_{\mathrm{vc}} = 0$), wherein IBI elimination is achieved by assuming that $L_{\mathrm{cp}} \geq L_h$ and discarding the first L_{cp} samples of $\widetilde{\mathbf{r}}(n)$ (i.e., the entire CP), it is sufficient to remove only L_h samples of the CP to achieve perfect IBI suppression[4]. This strategy is pursued by windowing receivers [5], [6], [8], [9] and, as we will see in the sequel, it allows one to gain additional degrees of freedom, which can also be exploited for NBI suppression. Interestingly, as pointed out in [11], [12], [13], [14], [15], perfect IBI elimination can be obtained also when $L_{\mathrm{cp}} < L_h$ (insufficient CP length), or even when $L_{\mathrm{cp}} = 0$ (*pure VC-based system*); in both cases, we will show that VC insertion is also mandatory to mitigate NBI effects.

In the rest of the paper, the following customary assumptions are considered: **(a1)** the information symbols $s(n)$ are modeled as a sequence of zero-mean independent and identically distributed (i.i.d.) circular random variables, with variance $\sigma_s^2 \triangleq \mathrm{E}[|s(n)|^2]$; **(a2)** the interference vector $\boldsymbol{\jmath}(n)$ is modeled as a zero-mean complex circular wide-sense stationary (WSS) random vector, statistically independent of $s(n)$; **(a3)** the noise vector $\mathbf{w}(n)$ is modeled as a zero-mean complex circular white Gaussian random vector, statistically independent of both $s(n)$ and $\boldsymbol{\jmath}(n)$, with autocorrelation matrix $\mathbf{R}_{\mathbf{ww}} \triangleq \mathrm{E}[\mathbf{w}(n)\,\mathbf{w}^H(n)] = \sigma_w^2\,\mathbf{I}_N$.

[2]Observe that VCs are commonly inserted at the edges of the spectrum to avoid aliasing problems at the receiver [1].

[3]Its inverse $\mathbf{W}_{\mathrm{DFT}} \triangleq \mathbf{W}^{-1}_{\mathrm{IDFT}} = \mathbf{W}^*_{\mathrm{IDFT}}$ defines the DFT matrix.

[4]Note that partial CP removal requires in principle *exact* knowledge of the channel order L_h. In practice, when only an upper bound $L_{\max} \geq L_h$ is available, one must resort to a suboptimal solution by discarding the first $L_{\max}$ samples of $\widetilde{\mathbf{r}}(n)$. Although the proposed method can work also when $L_{\max}$ is employed in the equalizer's synthesis (see Section V), for the sake of clarity, all the subsequent mathematical derivations are derived by assuming $L_{\max} = L_h$.

After partial CP removal, a linear zeroth-order[5] FIR equalizer $\mathbf{G} \triangleq [\mathbf{g}_0, \mathbf{g}_1, \ldots, \mathbf{g}_{Q-1}]^H \in \mathbb{C}^{Q\times N}$ is employed in order to jointly mitigate the interchannel interference (ICI), NBI and noise. The qth entry $y_q(n)$ of the equalizer output $\mathbf{y}(n) \triangleq [y_0(n), y_1(n), \ldots, y_{Q-1}(n)]^T = \mathbf{G}\,\mathbf{r}(n)$ is then quantized to the nearest (in terms of Euclidean distance) symbol to form the estimate of qth data substream $s_q(n)$, for any $q \in \{0, 1, \ldots, Q-1\}$. Since FIR-ZF equalizers cannot operate satisfactorily in NBI-contaminated OFDM systems [4], [6], [7], [16], [17], we consider hereinafter linear maximum-SINR optimization criteria, which offer a good compromise between performance and complexity. Specifically, the linear IBI-free *unconstrained* maximum-SINR optimization criterion consists of maximizing the output SINR at the qth subcarrier which, accounting for (1) and assumptions (a1)–(a3), can be written as

$$\mathrm{SINR}_q(\mathbf{g}_q) \triangleq \frac{\mathrm{E}[|\mathbf{g}_q^H\,\mathbf{f}_{0,q}\,s_q(n)|^2]}{\mathrm{E}[|\mathbf{g}_q^H\,\mathbf{d}_q(n)|^2]} = \frac{\sigma_s^2\,|\mathbf{g}_q^H\,\mathbf{f}_{0,q}|^2}{\mathbf{g}_q^H\mathbf{R}_{\mathbf{d}_q\mathbf{d}_q}\,\mathbf{g}_q}\,, \quad \forall q \in \{0,1,\ldots,Q-1\}\,, \tag{2}$$

where $\mathbf{f}_{0,q} \in \mathbb{C}^N$ denotes the $(q+1)$th column of the composite matrix $\mathbf{F}_0$ defined in (1), whereas

$$\mathbf{R}_{\mathbf{d}_q\mathbf{d}_q} \triangleq \mathrm{E}[\mathbf{d}_q(n)\,\mathbf{d}_q^H(n)] = \sigma_s^2\,\overline{\mathbf{F}}_{0,q}\,\overline{\mathbf{F}}_{0,q}^H + \mathbf{R}_{\boldsymbol{\jmath}\boldsymbol{\jmath}} + \sigma_w^2\,\mathbf{I}_N \in \mathbb{C}^{N\times N} \tag{3}$$

is the autocorrelation matrix of the vector $\mathbf{d}_q(n) \triangleq \overline{\mathbf{F}}_{0,q}\,\overline{\mathbf{s}}_q(n) + \boldsymbol{\jmath}(n) + \mathbf{w}(n) \in \mathbb{C}^N$, which collects the *overall* disturbance at the qth subcarrier, i.e., ICI, NBI and noise, with $\overline{\mathbf{s}}_q(n) \in \mathbb{C}^{Q-1}$ denoting the vector that includes all the elements of $\mathbf{s}(n)$ except for the $(q+1)$th entry $s_q(n)$ and $\overline{\mathbf{F}}_{0,q} \in \mathbb{C}^{N\times(Q-1)}$ denoting the matrix that includes all the columns of $\mathbf{F}_0$ except for the $(q+1)$th column $\mathbf{f}_{0,q}$, and, finally, $\mathbf{R}_{\boldsymbol{\jmath}\boldsymbol{\jmath}} \triangleq \mathrm{E}[\boldsymbol{\jmath}(n)\,\boldsymbol{\jmath}^H(n)] \in \mathbb{C}^{N\times N}$ is the autocorrelation matrix of $\boldsymbol{\jmath}(n)$. By resorting to the Cauchy-Schwartz's inequality [21], one has (see also [24]) that the optimal vector maximizing (2) is

$$\mathbf{g}_{q,\mathrm{opt}} = \varrho_q\,\mathbf{R}_{\mathbf{d}_q\mathbf{d}_q}^{-1}\,\mathbf{f}_{0,q}\,, \quad \text{with } \varrho_q \in \mathbb{C}-\{0\}, \tag{4}$$

and the corresponding SINR turns out to be $\mathrm{SINR}_{q,\mathrm{opt}} \triangleq \mathrm{SINR}_q(\mathbf{g}_{q,\mathrm{opt}}) = \sigma_s^2\,\mathbf{f}_{0,q}^H\,\mathbf{R}_{\mathbf{d}_q\mathbf{d}_q}^{-1}\,\mathbf{f}_{0,q}$. It is worth noting that, if the disturbance contribution at the qth equalizer output is a Gaussian random variable $\forall n \in \mathbb{Z}$, then $\mathbf{g}_{q,\mathrm{opt}}$ minimizes also the symbol error probability at the qth subcarrier [23].

III. Performance analysis of IBI-free unconstrained maximum-SINR equalizers

In this section, as a first step, the disturbance suppression capabilities of the maximum-SINR equalizer (4) are analyzed, under the ideal assumption that $\mathbf{R}_{\mathbf{d}_q\mathbf{d}_q}$ is perfectly known at the receiver. Since the performance of NBI-contaminated OFDM systems is mainly limited by IBI, ICI and NBI, we derive the analytical expression of $\mathrm{SINR}_{q,\mathrm{opt}}$ in the high signal-to-noise ratio (SNR) region, i.e., as σ_w^2 approaches to zero. Towards this aim, we rely on some results [25] regarding the approximate dimensionality of exactly time-limited and nominally band-limited signals, avoiding, therefore, to assume any explicit parametric model for the NBI. Specifically, let $\xi_1 \geq \xi_2 \geq \ldots \geq \xi_N$ and $\mathbf{u}_1, \mathbf{u}_2, \ldots, \mathbf{u}_N$ denote, respectively, the eigenvalues and the corresponding eigenvectors of the NBI autocorrelation matrix $\mathbf{R}_{\boldsymbol{\jmath}\boldsymbol{\jmath}}$ of the vector $\boldsymbol{\jmath}(n)$, obtained by collecting N samples from $\widetilde{\jmath}_c(t)$ and, moreover, let W_{nbi} be the (nominal) bandwidth of the narrowband process $\widetilde{\jmath}_c(t)$. It can be shown [25] that, for reasonably large[6] values of N, the first $R_{\mathrm{nbi}} \triangleq \lceil N\,T_c\,W_{\mathrm{nbi}}\rceil + 1$ eigenvalues $\xi_1, \xi_2, \ldots, \xi_{R_{\mathrm{nbi}}}$ turn out to be significantly different from zero, whereas the remaining ones $\xi_{R_{\mathrm{nbi}}+1}, \xi_{R_{\mathrm{nbi}}+2}, \ldots, \xi_N$ are vanishingly small. In the case of NBI, it happens in practice that, compared with the bandwidth of the multicarrier system, the bandwidth W_{nbi} is significantly smaller and, thus, it turns out that $R_{\mathrm{nbi}} \ll N$. Under this assumption, we provide the following Theorem:

Theorem 1: Let $H(z) \triangleq \sum_{n=0}^{L_h} h(n)\,z^{-n}$ and $\mathcal{I}_{\mathrm{uc}} \triangleq \{i_0, i_1, \ldots, i_{Q-1}\} \equiv \{0, 1, \ldots, M-1\} - \mathcal{I}_{\mathrm{vc}}$ denote the channel transfer function and the index set of the used subcarriers, respectively, and, let $\mathbf{U}_1 \triangleq [\mathbf{u}_1, \ldots, \mathbf{u}_{R_{\mathrm{nbi}}}] \in \mathbb{C}^{N\times R_{\mathrm{nbi}}}$ collect all the eigenvectors corresponding to the first R_{nbi} eigenvalues of $\mathbf{R}_{\boldsymbol{\jmath}\boldsymbol{\jmath}}$. In the limiting case of vanishingly small noise, the maximum-SINR equalizer (4) assures perfect ICI and NBI suppression ($\mathrm{SINR}_{q,\mathrm{opt}} \to +\infty$) for each used subcarrier if and only if (iff):

(c1) $N \geq Q + R_{\mathrm{nbi}}$;
(c2) $H(z)$ has no zero located at $z_i = e^{j\frac{2\pi}{M}i}$, with $i \in \mathcal{I}_{\mathrm{uc}}$;
(c3) $\mathcal{R}(\mathbf{F}_0) \cap \mathcal{R}(\mathbf{U}_1) = \{\mathbf{0}_N\}$.

Proof: See Appendix I. ∎

Some interesting remarks about Theorem 1 are now in order. First, condition (c1) admits a nice interpretation, by re-expressing it in the following form:

$$Q + M_{\mathrm{vc}} + (L_{\mathrm{cp}} - L_h) \geq Q + R_{\mathrm{nbi}} \Longleftrightarrow M_{\mathrm{vc}} + L_{\mathrm{cp}} \geq L_h + R_{\mathrm{nbi}}\,. \tag{5}$$

Observe that M_{vc} is the amount of frequency redundancy, whereas L_{cp} is the amount of time redundancy: hence, to allow for perfect ICI-plus-NBI suppression, the *overall* redundancy amount introduced in both domains must be no smaller than the sum of the channel order L_h and the NBI rank R_{nbi}. In the absence of NBI, i.e., when $R_{\mathrm{nbi}} = 0$, inequality (5) represents a necessary condition to allow for FIR-ZF equalization [12], [13], [14]. For pure CP-based systems (i.e., $M_{\mathrm{vc}} = 0$), eq. (5) is satisfied iff $L_{\mathrm{cp}} \geq L_h + R_{\mathrm{nbi}}$, that is, *the CP must be sufficiently longer than L_h and partial CP removal has to be performed at the receiver*. For pure VC-based systems (i.e., $L_{\mathrm{cp}} = 0$) or for hybrid CP/VC-based systems, either when the CP length is insufficient (i.e., $0 < L_{\mathrm{cp}} < L_h$) or when complete CP removal is performed at the receiver (i.e., $L_{\mathrm{cp}} = L_h$), eq. (5) requires that the number of VCs satisfy $M_{\mathrm{vc}} \geq (L_h - L_{\mathrm{cp}}) + R_{\mathrm{nbi}}$, hence, *a suitable amount of frequency-domain redundancy is mandatory in this case for achieving satisfactory ICI-plus-NBI cancellation*. Finally, for hybrid CP/VC-based systems with sufficient CP length (i.e., $L_{\mathrm{cp}} > L_h$), satisfactory NBI suppression can be achieved even

[5] The extension to a Kth-order FIR equalizer, which jointly elaborates $K+1$ OFDM symbols, is straightforward.

[6] Since $N = M + (L_{\mathrm{cp}} - L_h)$, this assumption is strictly verified only asymptotically, i.e., when the number M of subcarriers diverges.

when $M_{\rm vc} < R_{\rm nbi}$, provided that (c1) hold. Obviously, in practical (i.e., non asymptotic, see footnote 6) cases, for a given value of $L_{\rm cp} + M_{\rm vc}$, the actual performance depends on how the overall redundancy is distributed among the two domains. Furthermore, observe that assumption (c1) requires *only* upper bounds (rather than the exact knowledge) on the channel order L_h and the NBI rank $R_{\rm nbi}$ (i.e., the NBI bandwidth $W_{\rm nbi}$). In particular, it has been experimentally verified in [16] that, for practical values of N, the effective rank of the NBI turns out to be slightly greater than $R_{\rm nbi}$, and a quite conservative rule of thumb has been derived for determining the effective rank of the NBI, which can be used in (5).

As regards condition (c2), it should be observed that, in the case of pure CP-based systems, it reformulates the well-known result [22] that FIR-ZF equalizers do not exist if the channel transfer function $H(z)$ exhibits one or more zeros located in correspondence of the M subcarrier frequencies. On the other hand, for systems with VCs, as it was also recognized in [11], condition (c2) infers that VC insertion leads to milder restrictions on channel-zero locations, since possible zeros of $H(z)$ at the unused subcarrier frequencies do not affect the existence of FIR-ZF equalizers.

Condition (c3) is a technical requirement and imposes that the two subspaces $\mathcal{R}(\mathbf{F}_0)$ and $\mathcal{R}(\mathbf{U}_1)$ must be *nonoverlapping* or *disjoint*, which is less restrictive [26] than simple orthogonality between the same subspaces. To gain more insight about condition (c3), let us characterize the subspace $\mathcal{R}(\mathbf{F}_0)$ more explicitly. It is shown in Appendix II that the matrix $\mathbf{F}_0$ can be parameterized as

$$\mathbf{F}_0 = \boldsymbol{\mathcal{V}}_0 \, \boldsymbol{\Lambda}_0 \, \boldsymbol{\mathcal{H}}_{\rm uc} \, , \tag{6}$$

where $\boldsymbol{\mathcal{V}}_0 \triangleq [\boldsymbol{\zeta}_{i_0}, \boldsymbol{\zeta}_{i_1}, \ldots, \boldsymbol{\zeta}_{i_{Q-1}}] \in \mathbb{C}^{N \times Q}$ is a (rectangular) full-column rank Vandermonde matrix, with $\boldsymbol{\zeta}_{i_q} \triangleq [1, e^{j\frac{2\pi}{M} i_q}, e^{j\frac{4\pi}{M} i_q}, \ldots, e^{j\frac{2\pi}{M}(N-1) i_q}]^T \in \mathbb{C}^N$ being a Vandermonde vector, whereas the $Q \times Q$ diagonal matrices

$$\boldsymbol{\Lambda}_0 \triangleq \frac{1}{\sqrt{M}} \, {\rm diag}[e^{-j\frac{2\pi}{M}(L_{\rm cp}-L_h) i_0}, \ldots, e^{-j\frac{2\pi}{M}(L_{\rm cp}-L_h) i_{Q-1}}] \, , \tag{7}$$

and

$$\boldsymbol{\mathcal{H}}_{\rm uc} \triangleq {\rm diag}[H(e^{j\frac{2\pi}{M} i_0}), \ldots, H(e^{j\frac{2\pi}{M} i_{Q-1}})] \tag{8}$$

are nonsingular. Due to nonsingularity of $\boldsymbol{\Lambda}_0$ and $\boldsymbol{\mathcal{H}}_{\rm uc}$, it follows that $\mathcal{R}(\mathbf{F}_0) = \mathcal{R}(\boldsymbol{\mathcal{V}}_0)$: hence, under assumption (c2), *fulfillment of condition (c3) is independent of the desired channel impulse response*. As a matter of fact, it is also interesting to observe that, while $R_{\rm nbi}$ [and, hence, condition (c1)] does not depend on the spectral position of the NBI, the subspace $\mathcal{R}(\mathbf{U}_1)$ is instead influenced by the placement of the NBI within the OFDM spectrum. To clarify this fact, as in [27], let us consider a simple tone interference, whose baseband model is $\widetilde{\jmath}_c(t) = \alpha_I \, e^{j(2\pi f_I t + \theta)}$, where $\alpha_I \in \mathbb{R}$ is a deterministic amplitude, f_I represents the frequency offset from the carrier frequency, and θ is a random variable uniformly distributed in $[0, 2\pi)$. In this case, only one eigenvalue $\xi_1 = \alpha_I^2$ of the autocorrelation matrix of $\boldsymbol{\jmath}(n)$ is nonzero and, thus, one has $\mathbf{R}_{\boldsymbol{\jmath}\boldsymbol{\jmath}} = \alpha_I^2 \, \mathbf{u}_1 \, \mathbf{u}_1^H$, where $\mathbf{u}_1 \triangleq [1, e^{j2\pi f_I T_c}, \ldots, e^{j2\pi(N-1) f_I T_c}]^T \in \mathbb{C}^N$ is a Vandermonde vector. Therefore, in light of the aforementioned equivalence between $\mathcal{R}(\mathbf{F}_0)$ and $\mathcal{R}(\boldsymbol{\mathcal{V}}_0)$, condition (c3) imposes that the Vandermonde vector $\mathbf{u}_1$ must not belong to the column space of the Vandermonde matrix $\boldsymbol{\mathcal{V}}_0$. Relying on the properties of Vandermonde vectors [18], we can infer that this happens iff $e^{j2\pi f_I T_c} \neq e^{j\frac{2\pi}{M} i_q}$, $\forall q \in \{0, 1, \ldots, Q-1\}$, which, in its turn, imposes that $f_I T_c \neq \frac{i_q}{M} + m$, $\forall m \in \mathbb{Z}$. Remarkably, note that this last condition is violated when the tone interference is located exactly on a used subcarrier, i.e., $f_I = \frac{i_q}{M T_c}$, for $q \in \{0, 1, \ldots, Q-1\}$. Hence, *when a tone interference is located exactly on a used subcarrier, a maximum-SINR equalizer cannot completely suppress the disturbance (i.e., ICI-plus-NBI), even in the absence of noise*. As we will show in Section V, maximum-SINR equalizers exhibit this behavior for a nonnull-bandwidth NBI signal as well, when the NBI frequency offset is placed near to an used subcarrier.

In the sequel, we assume that conditions (c1), (c2) and (c3) are fulfilled. In practice, the synthesis of the maximum-SINR equalizer (4) requires that the disturbance autocorrelation matrix $\mathbf{R}_{\mathbf{d}_q \mathbf{d}_q}$ be consistently estimated from $\mathbf{r}(n)$, which contains also the contribution of the desired *signature* $\mathbf{f}_{0,q} \, s_q(n)$. On the other hand, it is well-known [24] that a maximum-SINR receiver can also be expressed in terms of the autocorrelation matrix $\mathbf{R}_{\mathbf{rr}} \triangleq {\rm E}[\mathbf{r}(n) \, \mathbf{r}^H(n)]$ of $\mathbf{r}(n)$, which can be estimated from the received data more easily than $\mathbf{R}_{\mathbf{d}_q \mathbf{d}_q}$. An equalizer belonging to the maximum-SINR family is the well-known MMSE one [23], which is the solution of the optimization problem

$$\begin{aligned} \mathbf{G}_{\rm mmse} &\triangleq [\mathbf{g}_{0,\rm mmse}, \mathbf{g}_{1,\rm mmse}, \ldots, \mathbf{g}_{Q-1,\rm mmse}]^H \\ &= \arg \min_{\mathbf{G} \in \mathbb{C}^{Q \times N}} {\rm E}[\|\mathbf{y}(n) - \mathbf{s}(n)\|^2] = \sigma_s^2 \, \mathbf{F}_0^H \, \mathbf{R}_{\mathbf{rr}}^{-1} \, , \end{aligned} \tag{9}$$

where $\mathbf{g}_{q,\rm mmse} = \sigma_s^2 \, \mathbf{R}_{\mathbf{rr}}^{-1} \, \mathbf{f}_{0,q}$, minimizes [24] the mean-square error ${\rm MSE}_q \triangleq {\rm E}[|y_q(n) - s_q(n)|^2]$ at the qth subcarrier, differs from $\mathbf{g}_{q,\rm opt}$ only for a complex nonzero scalar. The MMSE equalizer (9) was employed in [15], with reference to a pure VC-based OFDM system operating in a NBI-free scenario, in order to counteract the noise enhancement that is inherently associated with VC insertion [15]. To gain additional degrees of freedom for NBI suppression, an MMSE-based optimization criterion was also used in [7] for pure CP-based OFDM systems, by processing all the samples of the CP, i.e., without imposing the IBI-free constraint. Another well-known equalizer is the minimum mean-output-energy (MMOE) one [18] [also referred to [24] as the minimum variance distortionless response (MVDR) or Capon beamformer]:

$$\begin{aligned} \mathbf{g}_{q,\rm mmoe} &= (\mathbf{f}_{0,q}^H \, \mathbf{R}_{\mathbf{d}_q \mathbf{d}_q}^{-1} \, \mathbf{f}_{0,q})^{-1} \, \mathbf{R}_{\mathbf{d}_q \mathbf{d}_q}^{-1} \, \mathbf{f}_{0,q} \\ &= (\mathbf{f}_{0,q}^H \, \mathbf{R}_{\mathbf{rr}}^{-1} \, \mathbf{f}_{0,q})^{-1} \, \mathbf{R}_{\mathbf{rr}}^{-1} \, \mathbf{f}_{0,q} \, , \end{aligned} \tag{10}$$

which minimizes the ${\rm MOE}_q \triangleq {\rm E}[|y_q(n)|^2]$ at the qth subcarrier, subject to $\mathbf{g}_q^H \, \mathbf{f}_{0,q} = 1$, where the constraint prevents cancellation of the desired symbol. Similarly to the MMSE equalizer, the weight vector $\mathbf{g}_{q,\rm mmoe}$ also maximizes (2), since it differs from $\mathbf{g}_{q,\rm opt}$ for a complex nonzero scalar, with the second equality in (10) following from the matrix inversion lemma [21]. In matrix form, solution (10) can be expressed as $\mathbf{G}_{\rm mmoe} \triangleq [\mathbf{g}_{0,\rm mmoe}, \mathbf{g}_{1,\rm mmoe}, \ldots, \mathbf{g}_{Q-1,\rm mmoe}]^H =$

$[(\mathbf{F}_0^H\,\mathbf{R}_{\mathbf{rr}}^{-1}\,\mathbf{F}_0)\odot\mathbf{I}_Q]^{-1}\,\mathbf{F}_0^H\,\mathbf{R}_{\mathbf{rr}}^{-1}$ and, interestingly, by resorting to standard Lagrangian techniques, it can be shown that it turns out to be the solution of the constrained optimization criterion

$$\mathbf{G}_{\text{mmoe}} = \arg\min_{\mathbf{G}\in\mathbb{C}^{Q\times N}} \mathrm{E}[\|\mathbf{y}(n)\|^2]\,, \quad \text{subject to } \mathrm{diag}(\mathbf{G}\,\mathbf{F}_0) = [1,\ldots,1]^T\,. \tag{11}$$

Since $\mathbf{G}_{\text{mmse}}$ and $\mathbf{G}_{\text{mmoe}}$ are equivalent, in the sense that both maximize the output SINR at each subcarrier, we consider in the sequel the MMOE equalizer, because its analysis is simpler. Specifically, our aim is to investigate the SINR degradation when the filtering matrix $\mathbf{G}_{\text{mmoe}}$ is synthesized by using the sample correlation matrix $\widehat{\mathbf{R}}_{\mathbf{rr}}$ of $\mathbf{r}(n)$, estimated over K symbol intervals, rather than $\mathbf{R}_{\mathbf{rr}}$. In this situation, the weight vector (10) of the MMOE equalizer is

$$\widehat{\mathbf{g}}_{q,\text{mmoe}} = (\mathbf{f}_{0,q}^H\,\widehat{\mathbf{R}}_{\mathbf{rr}}^{-1}\,\mathbf{f}_{0,q})^{-1}\,\widehat{\mathbf{R}}_{\mathbf{rr}}^{-1}\,\mathbf{f}_{0,q}\,, \tag{12}$$

where, accounting for (1),

$$\widehat{\mathbf{R}}_{\mathbf{rr}} \triangleq \frac{1}{K}\sum_{n=0}^{K-1}\mathbf{r}(n)\,\mathbf{r}^H(n) = \widehat{\sigma}_{s_q}^2\,\mathbf{f}_{0,q}\,\mathbf{f}_{0,q}^H + \mathbf{f}_{0,q}\,\widehat{\mathbf{r}}_{\mathbf{d}_q s_q}^H + \widehat{\mathbf{r}}_{\mathbf{d}_q s_q}\,\mathbf{f}_{0,q}^H + \widehat{\mathbf{R}}_{\mathbf{d}_q\mathbf{d}_q}\,, \tag{13}$$

with $\widehat{\sigma}_{s_q}^2 \triangleq \frac{1}{K}\sum_{n=0}^{K-1}|s_q(n)|^2$, $\widehat{\mathbf{r}}_{\mathbf{d}_q s_q} \triangleq \frac{1}{K}\sum_{n=0}^{K-1}\mathbf{d}_q(n)\cdot s_q^*(n)$ and $\widehat{\mathbf{R}}_{\mathbf{d}_q\mathbf{d}_q} \triangleq \frac{1}{K}\sum_{n=0}^{K-1}\mathbf{d}_q(n)\,\mathbf{d}_q^H(n)$ representing sample estimates of the symbol variance σ_s^2, the cross-correlation between the disturbance vector $\mathbf{d}_q(n)$ and the desired symbol $s_q(n)$, and the autocorrelation matrix of $\mathbf{d}_q(n)$, respectively. In this case, the weight vector $\widehat{\mathbf{g}}_{q,\text{mmoe}}$ is random and, thus, the expectations in (2) must be evaluated also with respect to $\widehat{\mathbf{g}}_{q,\text{mmoe}}$, that is, $\mathrm{SINR}_q(\widehat{\mathbf{g}}_{q,\text{mmoe}}) = \sigma_s^2/\mathrm{E}_{\widehat{\mathbf{g}}_{q,\text{mmoe}},\mathbf{d}_q(n)}[|\widehat{\mathbf{g}}_{q,\text{mmoe}}^H\,\mathbf{d}_q(n)|^2]$, where we have additionally taken into account the constraint $\widehat{\mathbf{g}}_{q,\text{mmoe}}^H\,\mathbf{f}_{0,q} = 1$. By assuming[7] that $\widehat{\mathbf{g}}_{q,\text{mmoe}}$ is statistically independent of $\mathbf{d}_q(n)$ and resorting to the conditional expectation rule, one obtains $\mathrm{SINR}_q(\widehat{\mathbf{g}}_{q,\text{mmoe}}) = \sigma_s^2/\mathrm{E}_{\widehat{\mathbf{g}}_{q,\text{mmoe}}}[\widehat{\mathbf{g}}_{q,\text{mmoe}}^H\,\mathbf{R}_{\mathbf{d}_q\mathbf{d}_q}\,\widehat{\mathbf{g}}_{q,\text{mmoe}}]$. It is shown in [28] that, for moderate-to-high values of the sample size, i.e., $K \geq 3\,N$, the predominant cause of SINR degradation is represented by $\widehat{\mathbf{r}}_{\mathbf{d}_q s_q}$. Thus, after inserting (13) in (12) and, then, replacing $\widehat{\mathbf{R}}_{\mathbf{d}_q\mathbf{d}_q}$ with $\mathbf{R}_{\mathbf{d}_q\mathbf{d}_q}$, the weight vector $\widehat{\mathbf{g}}_{q,\text{mmoe}}$ can be approximated [28] as

$$\widehat{\mathbf{g}}_{q,\text{mmoe}} \simeq \mathbf{g}_{q,\text{mmoe}} - \mathbf{P}_q\,\mathbf{R}_{\mathbf{d}_q\mathbf{d}_q}^{-1}\,\widehat{\mathbf{r}}_{\mathbf{d}_q s_q}\,, \tag{14}$$

where

$$\mathbf{P}_q \triangleq \mathbf{I}_N - (\mathbf{f}_{0,q}^H\,\mathbf{R}_{\mathbf{d}_q\mathbf{d}_q}^{-1}\,\mathbf{f}_{0,q})^{-1}\,\mathbf{R}_{\mathbf{d}_q\mathbf{d}_q}^{-1}\,\mathbf{f}_{0,q}\,\mathbf{f}_{0,q}^H \in \mathbb{C}^{N\times N} \tag{15}$$

represents an oblique projection matrix and, under assumptions (a1)–(a3), the random vector $\widehat{\mathbf{r}}_{\mathbf{d}_q s_q}$ has zero-mean and autocorrelation matrix $\mathrm{E}[\widehat{\mathbf{r}}_{\mathbf{d}_q s_q}\,\widehat{\mathbf{r}}_{\mathbf{d}_q s_q}^H] = \frac{\sigma_s^2}{K}\,\mathbf{R}_{\mathbf{d}_q\mathbf{d}_q}$. Therefore, observing that $\sigma_s^2(\mathbf{g}_{q,\text{mmoe}}^H\,\mathbf{R}_{\mathbf{d}_q\mathbf{d}_q}\,\mathbf{g}_{q,\text{mmoe}})^{-1} = \mathrm{SINR}_{q,\text{opt}}$ and $\mathrm{trace}(\mathbf{R}_{\mathbf{d}_q\mathbf{d}_q}^{-1}\,\mathbf{P}_q\,\mathbf{R}_{\mathbf{d}_q\mathbf{d}_q}\,\mathbf{P}_q) = N-1$, one has

$$\mathrm{SINR}_q(\widehat{\mathbf{g}}_{q,\text{mmoe}}) \simeq \frac{\mathrm{SINR}_{q,\text{opt}}}{1+\frac{N-1}{K}\,\mathrm{SINR}_{q,\text{opt}}}\,. \tag{16}$$

By virtue of Theorem 1, it is interesting to note that, for practical values of K and for $\sigma_w^2 \to 0$, it results that $\mathrm{SINR}_{q,\text{opt}} \gg K/(N-1)$ and, thus, the expression (16) becomes $\mathrm{SINR}_q(\widehat{\mathbf{g}}_{q,\text{mmoe}}) \simeq K/(N-1)$, which shows that, due to the effects of the finite sample-size K, the SINR at the qth subcarrier saturates. This saturation effect gives rise to unacceptable bit-error-rate (BER) floors, when the value of K is not significantly larger than $N-1 = M+(L_{\text{cp}}-L_h)-1$. For instance, to achieve a SINR value of 10 dB at the qth subcarrier in the high SNR region, a sample size $K = 10\,(N-1)$ is required. On the other hand, for OFDM systems employing a large number M of subcarriers, imposing that $K \gg N-1$ requires very large values of the sample size which, in wireless scenarios, may lead to a packet duration exceeding the coherence time of the channel. To make the MMOE equalizer (12) robust against finite sample-size effects, one can exploit the eigenstructure of $\widehat{\mathbf{R}}_{\mathbf{rr}}$, obtaining thus a subspace-based implementation [29] of the receiver or, alternatively, resort to a diagonal loading approach [24], which consists of replacing in (12) matrix $\widehat{\mathbf{R}}_{\mathbf{rr}}^{-1}$ with $(\widehat{\mathbf{R}}_{\mathbf{rr}}+\gamma\,\mathbf{I}_N)^{-1}$, where γ denotes a diagonal loading factor. However, the former approach increases the receiver complexity and is not suited to simple adaptive implementations, whereas the optimal choice of γ in the latter approach is not a simple task, since it is scenario-dependent. In Section IV, we propose instead a constrained maximum-SINR receiver with channel estimation capabilities, which achieves a convenient tradeoff between ideal SINR performances and finite sample-size robustness.

In conclusion, it should be observed that the computational complexity of the MMOE (or MMSE) equalizer is essentially dominated by the inversion $\widehat{\mathbf{R}}_{\mathbf{rr}}^{-1}$, which requires $\mathcal{O}(N^3)$ flops, with $N = M + (L_{\text{cp}} - L_h)$. This computational burden might be prohibitive for OFDM systems employing a large number M of subcarriers and/or operating in time-varying NBI environments. In these scenarios, it is customary to resort to the recursive least square (RLS) algorithm [24], [30], which assures a fast symbol-by-symbol updating of the receiver, with $\mathcal{O}(N^2)$ computational complexity per iteration.

IV. IBI-FREE CONSTRAINED MAXIMUM-SINR OPTIMIZATION

We start from the *constrained* MMOE (CMMOE) formulation [17] for pure CP-based OFDM systems in the presence of NBI, wherein the equalizer's synthesis is carried out by minimizing the same objective function of (11), subject to the *ICI-free constraint*, namely

$$\mathbf{G}_{\text{cmmoe}} = \arg\min_{\mathbf{G}\in\mathbb{C}^{Q\times N}} \mathrm{E}[\|\mathbf{y}(n)\|^2]\,, \text{subject to } \mathbf{G}\,\mathbf{F}_0 = \mathbf{I}_Q\,, \tag{17}$$

whose solution is $\mathbf{G}_{\text{cmmoe}} \triangleq [\mathbf{g}_{0,\text{cmmoe}},\ \mathbf{g}_{1,\text{cmmoe}},\ \ldots,\mathbf{g}_{Q-1,\text{cmmoe}}]^H = (\mathbf{F}_0^H\,\mathbf{R}_{\mathbf{rr}}^{-1}\,\mathbf{F}_0)^{-1}\,\mathbf{F}_0^H\,\mathbf{R}_{\mathbf{rr}}^{-1}$. It is apparent that, while Q linear constraints are imposed in (11) for preserving the desired symbols $\{s_q(n)\}_{q=0}^{Q-1}$ at each used

[7] Since $\widehat{\mathbf{g}}_{q,\text{mmoe}}$ is estimated from $\{\mathbf{r}(\ell)\}_{\ell=0}^{K-1}$, it is statistically independent from $\mathbf{d}_q(n)$, provided that $n \geq K$.

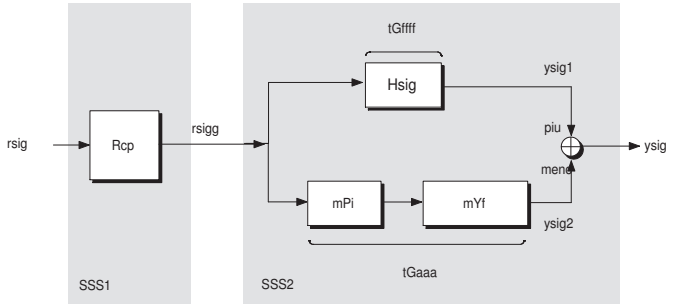

Fig. 1. Two-stage parallel implementation of the IBI-free CMMOE equalizer.

subcarrier, by treating the ICI in (1) in the same way as NBI and noise, the optimization problem (17) imposes Q^2 linear constraints, which not only preserve the desired symbols, but also assure *deterministic* ICI cancellation at each used subcarrier. The constrained optimization problem (17) can be reformulated as an unconstrained one, by resorting to an extension of the generalized sidelobe canceller decomposition [24], which was proposed in the array processing context. Specifically, following [17], it can be shown that $\mathbf{G}_{\text{cmmoe}}$ admits the canonical decomposition

$$\mathbf{G}_{\text{cmmoe}} = \underbrace{\mathbf{F}_0^{\dagger}}_{\mathbf{G}_{\text{cmmoe}}^{(\text{f})}} - \underbrace{\boldsymbol{\mathcal{Y}}_{\text{cmmoe}}\,\boldsymbol{\Pi}_0}_{\mathbf{G}_{\text{cmmoe}}^{(\text{a})}} = \mathbf{G}_{\text{cmmoe}}^{(\text{f})} - \mathbf{G}_{\text{cmmoe}}^{(\text{a})}, \quad (18)$$

with $\boldsymbol{\mathcal{Y}}_{\text{cmmoe}} \triangleq \mathbf{G}_{\text{cmmoe}}^{(\text{f})}\mathbf{R}_{\mathbf{rr}}\boldsymbol{\Pi}_0^H(\boldsymbol{\Pi}_0\mathbf{R}_{\mathbf{rr}}\boldsymbol{\Pi}_0^H)^{-1} = \mathbf{G}_{\text{cmmoe}}^{(\text{f})}\mathbf{R}_{\boldsymbol{\eta\eta}}\boldsymbol{\Pi}_0^H(\boldsymbol{\Pi}_0\mathbf{R}_{\boldsymbol{\eta\eta}}\boldsymbol{\Pi}_0^H)^{-1}$, where $\mathbf{G}_{\text{cmmoe}}^{(\text{f})} \in \mathbb{C}^{Q\times N}$ represents the minimum-norm (in the Frobenius sense) solution of the ICI-free constraint imposed in (17), whereas the *signal blocking matrix* $\boldsymbol{\Pi}_0 \in \mathbb{C}^{(N-Q)\times N}$ satisfies the relation $\boldsymbol{\Pi}_0\,\mathbf{F}_0 = \mathbf{O}_{(N-Q)\times Q}$. The choice of $\boldsymbol{\Pi}_0$ is not unique and will be discussed in Subsection IV-C. In the sequel, without loss of generality, we only impose that $\boldsymbol{\Pi}_0\,\boldsymbol{\Pi}_0^H = \mathbf{I}_{N-Q}$. The second equality in the expression of $\boldsymbol{\mathcal{Y}}_{\text{cmmoe}}$ is a direct consequence of the signal blocking property of $\boldsymbol{\Pi}_0$, with $\mathbf{R}_{\boldsymbol{\eta\eta}} \triangleq \mathbf{R}_{\boldsymbol{\jmath\jmath}} + \sigma_w^2\,\mathbf{I}_N \in \mathbb{C}^{N\times N}$ representing the autocorrelation matrix of the NBI-plus-noise vector $\boldsymbol{\eta}(n) \triangleq \boldsymbol{\jmath}(n) + \mathbf{w}(n)$. Decomposition (18) leads to the *two-stage* structure sketched in Fig. 1, which shows that the second stage $\mathbf{G}_{\text{cmmoe}}$ is the difference of a *fixed* (i.e., data-independent) term $\mathbf{G}_{\text{cmmoe}}^{(\text{f})}$ and a *free* or *adaptive* term $\mathbf{G}_{\text{cmmoe}}^{(\text{a})}$. Remarkably, in the absence of NBI, i.e., when $\mathbf{R}_{\boldsymbol{\jmath\jmath}} = \mathbf{O}_{N\times N}$, the adaptive part of the CMMOE equalizer vanishes, and $\mathbf{G}_{\text{cmmoe}}$ reduces to its data-independent part.

Since the CMMOE equalizer (17) has been obtained by adding further constraints to the matrix optimization problem (11), in the ideal situation when $\mathbf{R}_{\mathbf{rr}}$ is perfectly known, the CMMOE equalizer does not maximize the output SINR for each subcarrier. Our goal is to show that, with respect to the MMOE equalizer, the ICI-free constraint gains robustness against finite sample-size effects (Subsection IV-B), without compromising the ideal NBI suppression capabilities in the high SNR region (Subsection IV-A). Furthermore, we show that the CMMOE equalizer admits a computationally-efficient adaptive implementation, with embedded channel estimation capabilities (Subsection IV-C).

A. Ideal SINR analysis

On the basis of (18), it can be readily shown that the weight vector $\mathbf{g}_{q,\text{cmmoe}}$ corresponding to the qth subcarrier can be expressed as

$$\begin{aligned}\mathbf{g}_{q,\text{cmmoe}} &= \underbrace{(\mathbf{F}_0^{\dagger})^H\boldsymbol{\jmath}_q}_{\mathbf{g}_{q,\text{cmmoe}}^{(\text{f})}} - \boldsymbol{\Pi}_0^H\underbrace{(\boldsymbol{\Pi}_0\mathbf{R}_{\boldsymbol{\eta\eta}}\boldsymbol{\Pi}_0^H)^{-1}\boldsymbol{\Pi}_0\mathbf{R}_{\boldsymbol{\eta\eta}}\mathbf{g}_{q,\text{cmmoe}}^{(\text{f})}}_{\mathbf{g}_{q,\text{cmmoe}}^{(\text{a})}} \\ &= \mathbf{g}_{q,\text{cmmoe}}^{(\text{f})} - \boldsymbol{\Pi}_0^H\,\mathbf{g}_{q,\text{cmmoe}}^{(\text{a})}\,, \end{aligned} \quad (19)$$

where $\boldsymbol{\jmath}_q \triangleq [\overbrace{0,\ldots,0}^{q},1,0,\ldots,0] \in \mathbb{R}^Q$. It is worth noting that, accounting for (1), vector $\mathbf{g}_{q,\text{cmmoe}}$ turns out [24] to be the solution of the following constrained optimization problem

$$\begin{aligned}\mathbf{g}_{q,\text{cmmoe}} &= \arg\min_{\mathbf{g}_q\in\mathbb{C}^N} \mathrm{E}[|y_q(n)|^2]\,, \\ &\text{subject to} \quad \mathbf{g}_q^H\,\mathbf{f}_{0,q} = 1 \text{ and } \mathbf{g}_q^H\,\overline{\mathbf{F}}_{0,q} = \mathbf{0}_{Q-1}^T\,, \end{aligned} \quad (20)$$

where the goal of the first linear constraint is to preserve the desired symbol, whereas the remaining $Q-1$ linear constraints assure perfect ICI suppression at the qth subcarrier. Solution (20) is also known [24] as the linearly constrained minimum variance (LCMV) beamformer. As a consequence of the constraints in (20), the output SINR (2) of the CMMOE equalizer at the qth subcarrier can be written as $\text{SINR}_{q,\text{cmmoe}} \triangleq \text{SINR}_q(\mathbf{g}_{q,\text{cmmoe}}) = \sigma_s^2/\mathcal{P}_{q,\text{cmmoe}}$ where, accounting for (19),

$$\begin{aligned}\mathcal{P}_{q,\text{cmmoe}} &\triangleq \mathbf{g}_{q,\text{cmmoe}}^H\,\mathbf{R}_{\boldsymbol{\eta\eta}}\,\mathbf{g}_{q,\text{cmmoe}} \\ &= (\mathbf{g}_{q,\text{cmmoe}}^{(\text{f})})^H\,\mathbf{R}_{\boldsymbol{\eta\eta}}\,\mathbf{g}_{q,\text{cmmoe}}^{(\text{f})} - (\mathbf{g}_{q,\text{cmmoe}}^{(\text{f})})^H\,\mathbf{R}_{\boldsymbol{\eta\eta}}\,\boldsymbol{\Pi}_0^H \\ &\quad\cdot(\boldsymbol{\Pi}_0\,\mathbf{R}_{\boldsymbol{\eta\eta}}\,\boldsymbol{\Pi}_0^H)^{-1}\boldsymbol{\Pi}_0\,\mathbf{R}_{\boldsymbol{\eta\eta}}\,\mathbf{g}_{q,\text{cmmoe}}^{(\text{f})} \end{aligned} \quad (21)$$

represents the disturbance (NBI-plus-noise) power at the equalizer output. Observe that, from a mathematical point of view, because of the additional linear constraints $\mathbf{g}_q^H\,\overline{\mathbf{F}}_{0,q} = \mathbf{0}_{Q-1}^T$ imposed in (20), the output $\text{SINR}_{q,\text{cmmoe}}$ cannot be larger than the maximum value $\text{SINR}_{q,\text{opt}}$, i.e., $\text{SINR}_{q,\text{cmmoe}} \leq \text{SINR}_{q,\text{opt}}$. In other words, when the SOS of the received data are ideally known at the receiver, the CMMOE equalizer cannot perform better than the MMOE (or MMSE) equalizer. However, the following Theorem proves that, under conditions (c1), (c2) and (c3), similarly to a maximum-SINR equalizer, the CMMOE detector is able to completely reject the NBI as the noise variance σ_w^2 vanishes, that is, in the high SNR region, $\text{SINR}_{q,\text{cmmoe}}$ (approximatively) attains the maximum value $\text{SINR}_{q,\text{opt}}$.

Theorem 2: In the limiting situation of vanishingly small noise, the CMMOE equalizer (17) enables perfect NBI suppression for each used subcarrier, i.e., $\lim_{\sigma_w^2\to 0}\mathcal{P}_{q,\text{cmmoe}} = 0$, $\forall q \in \{0,1,\ldots,Q-1\}$, iff conditions (c1), (c2) and (c3) hold.

Proof: See Appendix III. ■

Besides confirming the statement of Theorem 2 for moderate-to-high values of the SNR, the simulation results of Section V will show moreover that, with respect to the MMOE equalizer, the performance penalty paid by the CMMOE equalizer is extremely small in the low SNR region. As a side comment, observe that, similarly to a maximum-SINR equalizer, the CMMOE cannot completely suppress a tone interference located exactly on a subcarrier, even in the

absence of noise, since in this case condition (c3) is violated. This is in agreement with the performance analysis carried out in [17] for pure CP-based OFDM systems. Furthermore, as it is shown in Section V, similarly to a maximum-SINR receiver, the CMMOE equalizer is not able to satisfactorily reject a nonnull-bandwidth NBI signal, when its frequency offset is placed near to a used subcarrier.

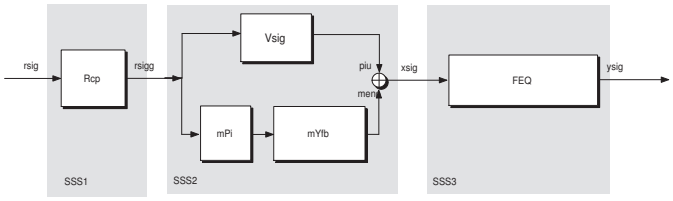

Fig. 2. Three-stage representation of the IBI-free CMMOE equalizer.

B. Performance analysis for finite sample-size

In this subsection, we evaluate the SINR degradation when the filtering matrix $\mathbf{G}_{\text{cmmoe}}$ is synthesized by using the sample correlation matrix $\widehat{\mathbf{R}}_{\mathbf{rr}}$ of $\mathbf{r}(n)$, given by (13). In this case, the estimate $\widehat{\mathbf{g}}_{q,\text{cmmoe}}$ of the weight vector (19) can be written as

$$\widehat{\mathbf{g}}_{q,\text{cmmoe}} = \mathbf{g}^{(\text{f})}_{q,\text{cmmoe}} - \mathbf{\Pi}_0^H (\mathbf{\Pi}_0 \widehat{\mathbf{R}}_{\mathbf{rr}} \mathbf{\Pi}_0^H)^{-1} \cdot \mathbf{\Pi}_0 \widehat{\mathbf{R}}_{\mathbf{rr}} \mathbf{g}^{(\text{f})}_{q,\text{cmmoe}} . \quad (22)$$

Reasoning as in Section III for $\widehat{\mathbf{g}}_{q,\text{mmoe}}$ and, moreover, taking into account the additional constraints $\widehat{\mathbf{g}}^H_{q,\text{cmmoe}} \overline{\mathbf{F}}_{0,q} = \mathbf{0}^T_{Q-1}$, one obtains $\text{SINR}_q(\widehat{\mathbf{g}}_{q,\text{cmmoe}}) = \sigma_s^2 / \text{E}_{\widehat{\mathbf{g}}_{q,\text{cmmoe}}}[\widehat{\mathbf{g}}^H_{q,\text{cmmoe}} \mathbf{R}_{\boldsymbol{\eta\eta}} \widehat{\mathbf{g}}_{q,\text{cmmoe}}]$. By substituting (13) in (22) and accounting for the signal blocking property of $\mathbf{\Pi}_0$, we obtain, after tedious but straightforward matrix algebra,

$$\widehat{\mathbf{g}}_{q,\text{cmmoe}} = \left[\mathbf{g}^{(\text{f})}_{q,\text{cmmoe}} - \mathbf{\Pi}_0^H (\mathbf{\Pi}_0 \widehat{\mathbf{R}}_{\boldsymbol{\eta\eta}} \mathbf{\Pi}_0^H)^{-1} \mathbf{\Pi}_0 \widehat{\mathbf{R}}_{\boldsymbol{\eta\eta}} \mathbf{g}^{(\text{f})}_{q,\text{cmmoe}}\right] - \mathbf{\Pi}_0^H (\mathbf{\Pi}_0 \widehat{\mathbf{R}}_{\boldsymbol{\eta\eta}} \mathbf{\Pi}_0^H)^{-1} \mathbf{\Pi}_0 \widehat{\mathbf{r}}_{\mathbf{d}_q s_q} , \quad (23)$$

with $\widehat{\mathbf{R}}_{\boldsymbol{\eta\eta}} \triangleq \frac{1}{K} \sum_{n=0}^{K-1} \boldsymbol{\eta}(n) \boldsymbol{\eta}^H(n)$ representing the sample estimate of the autocorrelation matrix of $\boldsymbol{\eta}(n)$. Eq. (23) evidences that $\widehat{\mathbf{g}}_{q,\text{cmmoe}}$ is composed of two terms: the former represents an estimate of $\mathbf{g}_{q,\text{cmmoe}}$ [see (19)], while the latter is the perturbation resulting from the nonzero sample cross-correlation vector $\widehat{\mathbf{r}}_{\mathbf{d}_q s_q}$. Along the same lines of Section III, we resort in (23) to the approximation

$$\widehat{\mathbf{g}}_{q,\text{cmmoe}} \simeq \mathbf{g}_{q,\text{cmmoe}} - \mathbf{\Pi}_0^H (\mathbf{\Pi}_0 \mathbf{R}_{\boldsymbol{\eta\eta}} \mathbf{\Pi}_0^H)^{-1} \mathbf{\Pi}_0 \widehat{\mathbf{r}}_{\mathbf{d}_q s_q} , \quad (24)$$

that is, we replace the sample autocorrelation matrix $\widehat{\mathbf{R}}_{\boldsymbol{\eta\eta}}$ with the exact one $\mathbf{R}_{\boldsymbol{\eta\eta}}$. Relying on (24) and accounting for $\mathbf{\Pi}_0 \mathbf{R}_{\mathbf{d}_q \mathbf{d}_q} \mathbf{\Pi}_0^H = \mathbf{\Pi}_0 \mathbf{R}_{\boldsymbol{\eta\eta}} \mathbf{\Pi}_0^H$, it is easily proven that

$$\text{SINR}_q(\widehat{\mathbf{g}}_{q,\text{cmmoe}}) \simeq \frac{\text{SINR}_{q,\text{cmmoe}}}{1 + \frac{N-Q}{K} \text{SINR}_{q,\text{cmmoe}}} . \quad (25)$$

A comparison between (16) and (25) is in order. First, note that, as a consequence of Theorem 2, for practical values of K and for $\sigma_w^2 \to 0$, it results that $\text{SINR}_{q,\text{cmmoe}} \gg K/(N-Q)$ and, thus, eq. (25) becomes $\text{SINR}_q(\widehat{\mathbf{g}}_{q,\text{cmmoe}}) \simeq K/(N-Q)$. Therefore, similarly to the MMOE equalizer (12), the SINR at the qth subcarrier of the CMMOE equalizer (22) saturates. However, the saturation value is higher than that of the MMOE equalizer: in fact, while $\text{SINR}_q(\widehat{\mathbf{g}}_{q,\text{mmoe}})$ approaches $K/(N-1)$ in the high SNR region, the SINR floor of the CMMOE equalizer is determined by $N-Q$, which is much smaller than $N-1$ since in OFDM systems of practical interest $Q \gg 1$. This implies that, to achieve a given target SINR as σ_w^2 approaches zero, the CMMOE equalizer (22) allows one to use a considerably smaller sample size $K_{\text{cmmoe}} = \frac{N-Q}{N-1} K_{\text{mmoe}}$ in comparison with that required by the MMOE equalizer (12). For instance, with reference to the HIPERLAN/2 context (channel model A) [31], wherein $Q = 52$, $M_{\text{vc}} = 12$, $L_{\text{cp}} = 16$ and $L_h \leq L_{\max} = 8$, it results that $\frac{N-1}{N-Q} \simeq 4$, i.e., K_{mmoe} must be four times larger than K_{cmmoe} to achieve the same performance. It is shown in Section V that the CMMOE equalizer (22) outperforms the MMOE one (12) also for low values of the SNR since, while $N-Q$ is significantly smaller than $N-1$ in practice, $\text{SINR}_{q,\text{cmmoe}}$ is only slightly inferior to $\text{SINR}_{q,\text{opt}}$ in the low-SNR region.

C. Three-stage implementation, computational complexity and channel acquisition

Before discussing computational complexity issues, we would like to highlight a further nice property of the CMMOE equalizer. By resorting to the parameterization (6) of $\mathbf{F}_0$, one obtains that, due to the nonsingularity of the diagonal matrices $\mathbf{\Lambda}_0$ and $\boldsymbol{\mathcal{H}}_{\text{uc}}$, the fixed term $\mathbf{G}^{(\text{f})}_{\text{cmmoe}}$ of $\mathbf{G}_{\text{cmmoe}}$ in (18) can be written as $\mathbf{G}^{(\text{f})}_{\text{cmmoe}} = (\boldsymbol{\mathcal{V}}_0 \mathbf{\Lambda}_0 \boldsymbol{\mathcal{H}}_{\text{uc}})^\dagger = \boldsymbol{\mathcal{H}}_{\text{uc}}^{-1} \mathbf{\Lambda}_0^{-1} \boldsymbol{\mathcal{V}}_0^\dagger$. Moreover, parameterization (6) leads to a *channel-independent* synthesis of the signal blocking matrix $\mathbf{\Pi}_0$. Indeed, under condition (c2), the null space of $\mathbf{\Pi}_0$ spans the column space of $\mathbf{F}_0$ which, in its turn, coincides with the column space of $\boldsymbol{\mathcal{V}}_0$, whose structure does not depend on the channel coefficients. Thus, the condition $\mathbf{\Pi}_0 \mathbf{F}_0 = \mathbf{O}_{(N-Q)\times Q}$ is equivalent to $\mathbf{\Pi}_0 \boldsymbol{\mathcal{V}}_0 = \mathbf{O}_{(N-Q)\times Q}$, that is, the synthesis of $\mathbf{\Pi}_0$ does not require knowledge of the channel vector $\mathbf{h} \triangleq [h(0), h(1), \ldots, h(L_h)]^T \in \mathbb{C}^{L_h+1}$ and, thus, together with the Moore-Penrose inverse of $\boldsymbol{\mathcal{V}}_0$, can be carried out *off-line* by resorting to any orthonormalization algorithm (e.g., QR or singular value decomposition), without requiring real-time extra computations. On the basis of these observations, we can rewrite (18) equivalently as follows

$$\mathbf{G}_{\text{cmmoe}} = \boldsymbol{\mathcal{H}}_{\text{uc}}^{-1} \mathbf{\Lambda}_0^{-1} \underbrace{(\boldsymbol{\mathcal{V}}_0^\dagger - \boldsymbol{\mathcal{Y}}^{(b)}_{\text{cmmoe}} \mathbf{\Pi}_0)}_{\mathbf{G}^{(\text{b})}_{\text{cmmoe}} \in \mathbb{C}^{Q\times N}} = \boldsymbol{\mathcal{H}}_{\text{uc}}^{-1} \mathbf{\Lambda}_0^{-1} \mathbf{G}^{(\text{b})}_{\text{cmmoe}} , \quad (26)$$

with $\boldsymbol{\mathcal{Y}}^{(b)}_{\text{cmmoe}} \triangleq \boldsymbol{\mathcal{V}}_0^\dagger \mathbf{R}_{\mathbf{rr}} \mathbf{\Pi}_0^H (\mathbf{\Pi}_0 \mathbf{R}_{\mathbf{rr}} \mathbf{\Pi}_0^H)^{-1} \in \mathbb{C}^{Q\times(N-Q)}$. Remarkably, synthesis of the matrix $\mathbf{G}^{(\text{b})}_{\text{cmmoe}}$ is completely *blind*, in the sense that it can be done relying only on the received data, without requiring knowledge of the channel vector $\mathbf{h}$. Additionally, it can be verified that $\mathbf{G}^{(\text{b})}_{\text{cmmoe}}$ turns out to be the solution of the following MOE-based criterion

$$\mathbf{G}^{(\text{b})}_{\text{cmmoe}} = \arg \min_{\mathbf{G}\in\mathbb{C}^{Q\times N}} \text{E}[\|\mathbf{y}(n)\|^2] , \text{subject to } \mathbf{G}\,\boldsymbol{\mathcal{V}}_0 = \mathbf{I}_Q . \quad (27)$$

As it is apparent, the difference between (17) and (27) lies in the imposed (matrix) constraint. Specifically, with reference to (1), the constraint in (17) is aimed at preserving the

desired symbol vector $\mathbf{s}(n)$ while minimizing the output power and, at the same time, at deterministically suppressing the ICI. On the other hand, the constraint in (27) has the only goal of blindly preserving $\mathbf{s}(n)$ during the minimization of the mean output power, by assuring that $\mathbf{G}_{\text{cmmoe}}^{(\text{b})}\,\mathbf{F}_0\,\mathbf{s}(n) = \mathbf{\Lambda}_0\,\boldsymbol{\mathcal{H}}_{\text{uc}}\,\mathbf{s}(n)$. Decomposition (26) leads to the *three-stage* structure depicted in Fig. 2. The first stage assures blind deterministic IBI suppression, by requiring only the knowledge of an upper bound $L_{\max}$ on the channel order L_h. The filtering process carried out in the second stage by the matrix $\mathbf{G}_{\text{cmmoe}}^{(\text{b})}$ is basically aimed at blindly suppressing the NBI contribution, by means of a SOS-based processing, without distorting the desired symbol vector and without requiring knowledge of the channel impulse response. Finally, the task of the third stage is to perform one-tap deterministic FEQ for the used subcarriers by means of the diagonal matrix $\boldsymbol{\mathcal{H}}_{\text{uc}}^{-1}\,\mathbf{\Lambda}_0^{-1}$, based on the knowledge or estimation of the channel vector $\mathbf{h}$.

With respect to the conventional FFT-based ZF receiver, the proposed three-stage equalizer is more complex. However, this shortcoming is common to any reception technique (like, e.g., [5], [6], [8], [9], [16], [17]) which, unlike the conventional FFT-based ZF receiver, operates satisfactorily in the presence of a strong NBI. The main on-line computational burden of the CMMOE equalizer lies in the synthesis of $\boldsymbol{\mathcal{Y}}_{\text{cmmoe}}^{(b)}$, which must be estimated from the received data. When the direct-matrix-inversion (DMI) approach is employed (i.e., $\mathbf{R}_{\mathbf{rr}}$ in $\boldsymbol{\mathcal{Y}}_{\text{cmmoe}}^{(b)}$ is replaced by $\widehat{\mathbf{R}}_{\mathbf{rr}}$), this computational load is dominated by the inversion of $\mathbf{\Pi}_0\,\widehat{\mathbf{R}}_{\mathbf{rr}}\,\mathbf{\Pi}_0^H \in \mathbb{C}^{(N-Q)\times(N-Q)}$, which entails $\mathcal{O}[(N-Q)^3]$ flops, with $N-Q = M_{\text{vc}} + (L_{\text{cp}} - L_h)$. Hence, the computational complexity of the CMMOE equalizer is significantly smaller than that of the MMOE equalizer, since it depends on the number $M_{\text{vc}} \ll M$ of VCs instead of the number M of subcarriers. However, the DMI implementation of the CMMOE equalizer can be used only if, during the OFDM packet duration, the SOS of the NBI do not change significantly. When this condition is violated, one can resort to a recursive implementation of the CMMOE equalizer, wherein an estimate $\widehat{\boldsymbol{\mathcal{Y}}}_{\text{cmmoe}}^{(b)}$ of $\boldsymbol{\mathcal{Y}}_{\text{cmmoe}}^{(b)}$ is obtained from the incoming received data through symbol-by-symbol updating. Similarly to the RLS algorithm [30], after some calculations, it can be shown that the recursion for estimating $\boldsymbol{\mathcal{Y}}_{\text{cmmoe}}^{(b)}$ is

$$\widehat{\boldsymbol{\mathcal{Y}}}_{\text{cmmoe}}^{(b)}(n) = \widehat{\boldsymbol{\mathcal{Y}}}_{\text{cmmoe}}^{(b)}(n-1) + \left[\boldsymbol{\mathcal{V}}_0^{\dagger}\,\mathbf{r}(n) - \widehat{\boldsymbol{\mathcal{Y}}}_{\text{cmmoe}}^{(b)}(n-1)\,\mathbf{q}(n)\right]\,\mathbf{k}^H(n)\,, \quad (28)$$

where $\mathbf{k}(n) \triangleq [\lambda + \mathbf{q}^H(n)\,\mathbf{T}(n-1)\,\mathbf{q}(n)]^{-1}\,\mathbf{T}(n-1)\,\mathbf{q}(n) \in \mathbb{C}^{(N-Q)\times N}$ is the *overall gain* vector, and $\mathbf{q}(n) \triangleq \mathbf{\Pi}_0\,\mathbf{r}(n) \in \mathbb{C}^{(N-Q)\times N}$, with $\mathbf{T}(n)$ and $\lambda \in (0,1]$ denoting the estimate, at iteration n, of $[\mathbf{\Pi}_0\,\mathbf{R}_{\mathbf{rr}}(n)\,\mathbf{\Pi}_0^H]^{-1}$ and the forgetting factor of the recursive algorithm, respectively. According to the usual initialization strategy for the RLS algorithm, we set $\mathbf{T}(-1) = \delta^{-1}\,\mathbf{I}_{N-Q}$ and $\widehat{\boldsymbol{\mathcal{Y}}}_{\text{cmmoe}}^{(b)}(-1) = \mathbf{O}_{Q\times(N-Q)}$, where $\delta \in \mathbb{R}$ is a positive constant. By resorting to standard analysis tools [30], it can be proved that, as n grows, matrix $\widehat{\boldsymbol{\mathcal{Y}}}_{\text{cmmoe}}^{(b)}(n)$ converges in mean square to the optimal matrix $\boldsymbol{\mathcal{Y}}_{\text{cmmoe}}^{(b)}$, regardless of the eigenstructure of $\mathbf{R}_{\mathbf{rr}}$. Finally, it is worth noting that the recursive equation (28) requires a computational complexity per iteration of order only $\mathcal{O}[(N-Q)^2]$. In conclusion, we can infer that, unlike the IBI-free maximum-SINR equalizer, both the actual performance and the computational load of the IBI-free CMMOE equalizer depend on $N-Q = M_{\text{vc}} + (L_{\text{cp}} - L_h)$, whose value for OFDM systems of practical interest is remarkably less than N and, moreover, unlike the PTEQ-based approaches of [8], [9], is independent of the number Q of used subcarriers.

Hitherto, the channel vector $\mathbf{h}$ has been assumed to be exactly known. For the scenario at hand, the channel estimation task is dramatically complicated by the presence of the NBI, which renders conventional channel estimation techniques [19] not directly applicable. The three-stage decomposition (26) of the CMMOE equalizer is also instrumental for synthesizing a NBI-resistant channel estimation algorithm. Indeed, decomposition (26) evidences that, under conditions (c1)–(c3), IBI and NBI can be suppressed in the first and second stage, respectively, without requiring knowledge of the desired channel impulse response. In particular, as a consequence of Theorem 2, unless very severe noise is present, the output $\mathbf{x}(n) = [x_0(n), x_1(n), \ldots, x_{Q-1}(n)]^T \triangleq \mathbf{G}_{\text{cmmoe}}^{(\text{b})}\,\mathbf{r}(n) \in \mathbb{C}^Q$ of the second stage turns out to be nearly NBI-free and, thus, can be approximatively written as

$$\mathbf{x}(n) = \mathbf{\Lambda}_0\,\boldsymbol{\mathcal{H}}_{\text{uc}}\,\mathbf{s}(n) + \mathbf{v}(n)\,, \quad (29)$$

where $\mathbf{v}(n) = [v_0(n), v_1(n), \ldots, v_{Q-1}(n)]^T \triangleq \mathbf{G}_{\text{cmmoe}}^{(\text{b})}\,\mathbf{w}(n) \in \mathbb{C}^Q$ is the filtered noise vector. According to [19], it is assumed that $R \leq Q$ known symbols are inserted at known subcarrier locations $\mathcal{I}_{\text{p}} \triangleq \{p_0, p_1, \ldots, p_{R-1}\} \subset \mathcal{I}_{\text{uc}}$, for a given time index $\overline{n} \in \{0, 1, \ldots, K-1\}$. Denoting by $\overline{\mathbf{x}} \triangleq [x_{p_0}(\overline{n}), x_{p_1}(\overline{n}), \ldots, x_{p_{R-1}}(\overline{n})]^T \in \mathbb{C}^R$ and $\overline{\mathbf{v}} \triangleq [v_{p_0}(\overline{n}), v_{p_1}(\overline{n}), \ldots, v_{p_{R-1}}(\overline{n})]^T \in \mathbb{C}^R$ the vectors containing the entries of $\mathbf{x}(\overline{n})$ and $\mathbf{v}(\overline{n})$ at the pilot locations, respectively, we get

$$\overline{\mathbf{x}} = \mathbf{\Psi}\,\boldsymbol{\mathcal{W}}\,\mathbf{h} + \overline{\mathbf{v}}\,, \quad (30)$$

where

$$\mathbf{\Psi} \triangleq \frac{1}{\sqrt{M}}\,\text{diag}[s_{p_0}(\overline{n})\,e^{-j\frac{2\pi}{M}(L_{\text{cp}}-L_h)p_0}, \ldots, s_{p_{R-1}}(\overline{n})\,e^{-j\frac{2\pi}{M}(L_{\text{cp}}-L_h)p_{R-1}}] \in \mathbb{C}^{R\times R} \quad (31)$$

is a *nonsingular* diagonal matrix collecting all the pilot symbols, whereas the $[\boldsymbol{\mathcal{W}}]_{i,\ell}$ entry of the matrix $\boldsymbol{\mathcal{W}} \in \mathbb{C}^{R\times(L_h+1)}$ is $[\boldsymbol{\mathcal{W}}]_{i,\ell} = e^{-j2(\pi/N)i\ell}$, for $i \in \mathcal{I}_{\text{p}}$ and $\ell \in \{0, 1, \ldots, L_h\}$. To allow $\boldsymbol{\mathcal{W}}$ to be full-column rank, we assume that the number of pilot symbols is larger than channel memory, i.e., $R \geq L_h + 1$. It is worth noting that, due to filtering carried out in the second stage through the matrix $\mathbf{G}_{\text{cmmoe}}^{(\text{b})}$, accounting for the assumption (a3), the complex circular Gaussian noise vector $\overline{\mathbf{v}}$ turns out to be colored with zero-mean and autocorrelation matrix $\text{E}[\overline{\mathbf{v}}\,\overline{\mathbf{v}}^H] = \sigma_w^2\,\mathbf{\Xi}\,\mathbf{\Xi}^H$, where $\mathbf{\Xi} \in \mathbb{C}^{R\times N}$ is obtained from $\mathbf{G}_{\text{cmmoe}}^{(\text{b})}$ by picking up its rows at the pilot locations $\mathcal{I}_{\text{p}}$. Therefore, the maximum likelihood estimation (MLE) of $\mathbf{h}$ is given by (see [32])

$$\widehat{\mathbf{h}}_{\text{mle}} = \left[\boldsymbol{\mathcal{W}}^H\,\mathbf{\Psi}^*(\mathbf{\Xi}\,\mathbf{\Xi}^H)^{-1}\,\mathbf{\Psi}\,\boldsymbol{\mathcal{W}}\right]^{-1}\,\boldsymbol{\mathcal{W}}^H\,\mathbf{\Psi}^*(\mathbf{\Xi}\,\mathbf{\Xi}^H)^{-1}\,\overline{\mathbf{x}}\,. \quad (32)$$

$$\boldsymbol{\mathcal{W}}_{\text{redfern}} = \begin{bmatrix} \overline{\boldsymbol{\mathcal{Y}}}_1 & \mathbf{I}_{M-L_{\text{cp}}+L_h} & -\overline{\boldsymbol{\mathcal{Y}}}_1 \\ \frac{1}{2}\mathbf{I}_{L_{\text{cp}}-L_h} + \overline{\boldsymbol{\mathcal{Y}}}_2 & \mathbf{O}_{(L_{\text{cp}}-L_h)\times(M-L_{\text{cp}}+L_h)} & \frac{1}{2}\mathbf{I}_{L_{\text{cp}}-L_h} - \overline{\boldsymbol{\mathcal{Y}}}_2 \end{bmatrix} \tag{33}$$

Remarkably, it results [32] that $\widehat{\mathbf{h}}_{\text{mle}}$ is unbiased (i.e., $\text{E}[\widehat{\mathbf{h}}_{\text{mle}}] = \mathbf{h}$) and consistent (i.e., attains the Cramer-Rao lower bound) and, hence, it represents the minimum variance unbiased (MVU) estimator. After estimating $\mathbf{h}$ through (32), the third stage performs in practice the FEQ reported in Fig. 2 by resorting to the inverse of the diagonal matrix $\widehat{\boldsymbol{\mathcal{H}}}_{\text{uc}}$, whose entries are given by the transfer function of the estimated channel $\widehat{\mathbf{h}}_{\text{mle}}$, evaluated at $\{e^{j\frac{2\pi}{M}i_q}\}_{q=0}^{Q-1}$. A final remark concerns the computational complexity of the MLE estimator (32); since $R \geq L_h + 1$, the computational complexity of (32) is essentially dominated by the inversion of $\boldsymbol{\Xi}\,\boldsymbol{\Xi}^H$, which requires $\mathcal{O}(R^3)$ flops.

D. Relationships with existing NBI-resistant receivers

Receiver windowing [8], [9], [5], [6] is a low-complexity ZF equalization technique proposed for pure CP-based OFDM systems (i.e., $L_{\text{cp}} > 0$ and $M_{\text{vc}} = 0$). We focus attention here on the windowing receiver proposed by Redfern [6], since relationships with other windowing-based techniques can be established with similar reasonings. After some algebra, the equalizer of [6] can be expressed as $\mathbf{G}_{\text{redfern}} = \boldsymbol{\mathcal{H}}_{\text{uc}}^{-1}\,\mathbf{W}_{\text{DFT}}\,\boldsymbol{\mathcal{W}}_{\text{redfern}}$, where $\boldsymbol{\mathcal{W}}_{\text{redfern}}$, which is of the form shown by (33) at the top of the page, can be interpreted as a generalized windowing matrix, with $\overline{\boldsymbol{\mathcal{Y}}}_1 \in \mathbb{C}^{(M-L_{\text{cp}}+L_h)\times(L_{\text{cp}}-L_h)}$ and $\overline{\boldsymbol{\mathcal{Y}}}_2 \in \mathbb{C}^{(L_{\text{cp}}-L_h)\times(L_{\text{cp}}-L_h)}$. Note that, instead of the parallel implementation depicted in Fig. 1, matrix $\mathbf{G}_{\text{redfern}}$ leads to a *serial* decomposition of the ZF receiver and performs, in the given order, generalized windowing, DFT, and one-tap FEQ on the IBI-free received signal $\mathbf{r}(n)$. The windowing strategy of [6], as depicted in [6, Fig. 2], can be obtained from (33) by imposing $\overline{\boldsymbol{\mathcal{Y}}}_1 = \mathbf{O}_{(M-L_{\text{cp}}+L_h)\times(L_{\text{cp}}-L_h)}$ and $\overline{\boldsymbol{\mathcal{Y}}}_2 = \text{diag}(\overline{\mathbf{y}}_2)$, with $\overline{\mathbf{y}}_2 \in \mathbb{C}^{L_{\text{cp}}-L_h}$. In [6], vector $\overline{\mathbf{y}}_2$ is chosen so as to suppress the disturbance contribution in the MMSE sense, and its synthesis does not require *a priori* knowledge of the disturbance autocorrelation function. It is thus apparent that, in comparison with the CMMOE equalizer, although the technique of [6] allows one to reduce the implementation complexity (in terms of number of complex multiplications needed), the resulting equalizer has a diminished interference suppression capability, since the structure imposed to $\overline{\boldsymbol{\mathcal{Y}}}_1$ and $\overline{\boldsymbol{\mathcal{Y}}}_2$, before carrying out MMSE optimization, leads to *suboptimal* exploitation of the available degrees of freedom for disturbance suppression. It has been experimentally shown in [17] that, in comparison with the CMMOE equalizer, which fully exploits the available degrees of freedom, the receiver of [6] exhibits a substantial BER performance degradation and outperforms the conventional ZF receiver only slightly.

In [16], the authors considered an OFDM system with CP (i.e., $L_{\text{cp}} > L_h$), possibly employing VC insertion at the transmitting side[8] The receiver proposed in [16] is a two-stage IBI-free receiver, where the first stage removes the entire CP, by performing a fixed time-domain windowing. After some straightforward manipulations, it can be shown that the second stage $\mathbf{G}_{\text{nsl}} \in \mathbb{C}^{Q\times M}$ of [16] can be decomposed as $\mathbf{G}_{\text{nsl}} = \mathbf{G}_{\text{nsl}}^{(\text{f})} - \mathbf{G}_{\text{nsl}}^{(\text{a})}$, where[9] the fixed matrix $\mathbf{G}_{\text{nsl}}^{(\text{f})}$ satisfies the ICI-free equation, whereas the synthesis of $\mathbf{G}_{\text{nsl}}^{(\text{a})}$ requires knowledge of the autocorrelation matrix of the NBI. Although the receiver of [16] can work in a mismatched mode, its performance may degrade significantly if $\mathbf{R}_{\jmath\jmath}$ is not accurately known. In contrast, the proposed CMMOE strategy overcomes this drawback, since it does not require any *a priori* information about the NBI, but rather it implicitly estimates its SOS on the basis only of the received data. Furthermore, by virtue of the above decomposition of $\mathbf{G}_{\text{nsl}}$, it can be observed that the equalizer of [16] admits a parallel implementation, which is similar to that reported in Fig. 1. More specifically, the fixed filtering matrix $\mathbf{G}_{\text{nsl}}^{(\text{f})}$ performs substantially the same operations as $\mathbf{G}_{\text{cmmoe}}^{(\text{f})}$ in (18). Thus, similarly to the CMMOE equalizer, the upper branch of the receiver [16] contains both the OFDM signal and the disturbance. On the other hand, unlike $\mathbf{G}_{\text{cmmoe}}^{(\text{a})}$ in (18), *the adaptive filtering matrix* $\mathbf{G}_{\text{nsl}}^{(\text{a})}$ *does not exhibit in general the signal blocking property*. Indeed, for a system employing VC insertion at the transmitter (i.e., $M_{\text{vc}} > 0$), under the assumption that the M_{vc} subcarriers are located in the proximity of the NBI carrier frequency, the matrix $\mathbf{G}_{\text{nsl}}^{(\text{a})}$ behaves as a blocking matrix, which removes the OFDM signal component in the lower branch. On the other hand, when no VC insertion is carried out at the transmitter (i.e., $M_{\text{vc}} = 0$), matrix $\mathbf{G}_{\text{nsl}}^{(\text{a})}$ does not block the OFDM signal, and, thus, in addition to the disturbance contribution, the lower branch also contains the OFDM signal component. This is a very undesired situation, since subtraction between the upper and lower branch outputs leads to partial OFDM signal cancellation which, as observed in [16], implies a substantial performance degradation, in comparison with the case where VCs are available. On the contrary, the proposed CMMOE equalizer does not suffer of this problem.

V. Simulations results

In all the simulations, the parameters of the OFDM system have been chosen in accordance with the HIPERLAN/2 broadband wireless communication standard [31]. For this system, the number of subcarriers is $M = 64$ and the CP length is $L_{\text{cp}} = 16$, implying thus $P = M + L_{\text{cp}} = 80$. The sampling and the symbol periods are equal to $T_c = 50$ ns and $T = PT_c = 4$ μs, leading thus to a bandwidth of

[8]Although the equalizer of [16] can jointly elaborate multiple consecutive OFDM symbols, for the sake of comparison, we consider here a zeroth-order equalizer, which is the case examined in depth in the simulations reported in [16].

[9]For the sake of conciseness, we defer directly to [16] for the explicit expression of $\mathbf{G}_{\text{nsl}}^{(\text{f})}$ and $\mathbf{G}_{\text{nsl}}^{(\text{a})}$.

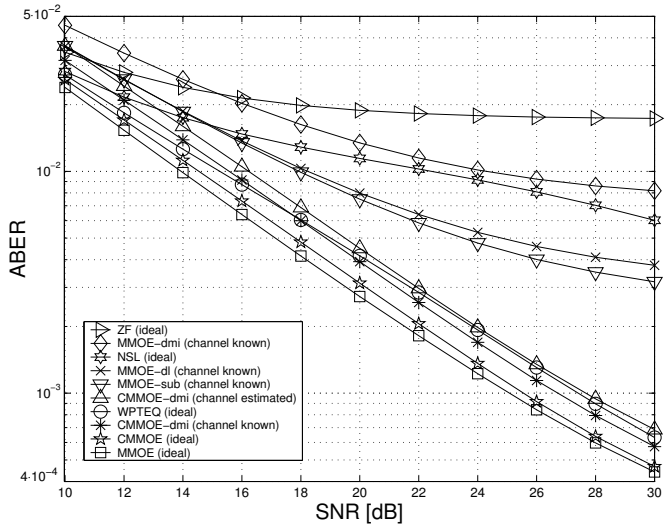

Fig. 3. ABER versus SNR (SIR $= 10$ dB, $K = 500$ symbols).

about 20 MHz. The number of VCs is $M_{\rm vc} = 12$, six of which are set at the beginning of the OFDM spectrum, five at the end, and one in correspondence of the center, i.e., $\mathcal{I}_{\rm vc} = \{0, 1, 2, 3, 4, 5, 32, 59, 60, 61, 62, 63\}$. As regards to the $Q = 52$ used subcarriers, those belonging to $\mathcal{I}_{\rm p} = \{11, 25, 39, 53\}$ carry QPSK training symbols, whereas the other ones convey the information-bearing sequences $\{s_q(n)\}_{q=0}^{Q-1}$, which have been drawn from a QPSK constellation. The channel impulse response $h_c(t)$ has been chosen according to the channel model A (see [31] for details), which corresponds to a typical office environment; in this case, the channel order L_h turns out to be less than or equal to $L_{\max} = 8$. As regards to the NBI, the baseband continuous-time $\widetilde{\jmath}_c(t)$ is modeled as a digitally modulated QPSK signal $\widetilde{\jmath}_c(t) = \sum_{k=-\infty}^{+\infty} s_I(k)\, \psi_I(t - k\, T_I)\, e^{\jmath 2\pi f_I t}$, where $T_I = T$ and, unless otherwise specified, the carrier frequency-offset f_I (measured with respect to the carrier frequency of the OFDM signal) is set to $f_I = \frac{13.5}{M\, T_c}$, whereas $\psi_I(t)$ is a Nyquist-shaped pulse with 30% excess bandwidth [23], which is truncated in the interval $(-5\, T_I, 5\, T_I)$; in this case, the power spectral density of $\widetilde{\jmath}_c(t)$ is essentially concentrated in a spectral band of width $W_{\rm nbi} = 325$ kHz. The additive noise vector $\mathbf{w}(n)$ has been modeled in accordance with (a3), and, on the basis of (1), the SNR and the signal-to-interference ratio (SIR) have been defined as SNR $\triangleq \mathrm{E}[\|\mathbf{F}_0\, \mathbf{s}(n)\|^2]/\mathrm{E}[\|\mathbf{w}(n)\|^2]$ and SIR $\triangleq \mathrm{E}[\|\mathbf{F}_0\, \mathbf{s}(n)\|^2]/\mathrm{E}[\|\boldsymbol{\jmath}(n)\|^2]$. In the following, we present the results of Monte Carlo computer simulations and compare them with the analytical results derived in Sections III and IV. Specifically, in addition to the data-estimated MMOE and CMMOE equalizers[10] given by (12) and (22) [referred to as "MMOE-dmi (channel known)" and "CMMOE-dmi (channel known)"], and their ideal counterparts [referred to as "MMOE (ideal)" and "CMMOE (ideal)"], we have considered the three-stage implementation (26) of the CMMOE equalizer [referred to as "CMMOE-dmi (channel estimated)"], wherein the estimate $\widehat{\boldsymbol{\mathcal{Y}}}_{\rm cmmoe}^{(b)}$ of $\boldsymbol{\mathcal{Y}}_{\rm cmmoe}^{(b)}$ is performed by using $\widehat{\mathbf{R}}_{\mathbf{rr}}$, and the channel vector $\mathbf{h}$ is estimated by resorting to (32) and relying only on the knowledge of the first symbol block $\mathbf{s}(0)$, which contains $R = Q$ pilot symbols, obtained by transmitting the same known symbol on all the used subcarriers, i.e., $\mathcal{I}_{\rm p} = \mathcal{I}_{\rm uc}$. Moreover, for the sake of comparison, we have also reported the performances of the following receivers[11]: the (data-independent) conventional ZF receiver [referred to as "ZF (ideal)"]; the subspace-based implementation [29] of the MMOE receiver [referred to as "MMOE-sub (channel known)"]; the diagonal loading version of the MMOE equalizer [referred to as "MMOE-dl (channel known)"], wherein the diagonal loading factor γ is optimally calculated as described in [24]; the receiver of [16] [referred to as "NSL (ideal)"], which has been synthesized by assuming exact knowledge of $\mathbf{h}$, $\mathbf{R}_{\boldsymbol{\jmath}\boldsymbol{\jmath}}$ and σ_w^2; the receiver of [9] [referred to as "WPTEQ (ideal)"], which has been synthesized by assuming[12] exact knowledge of $\mathbf{h}$ and $\mathbf{R}_{\mathbf{rr}}$.

As (overall) performance measure, in addition to the average SINR defined as ASINR $\triangleq \frac{1}{Q}\sum_{q=0}^{Q-1} \mathrm{SINR}_q$, with SINR_q being the output SINR at the qth used subcarrier [see also (2)], we have resorted to the average BER (ABER) defined as ABER $\triangleq \frac{1}{Q}\sum_{q=0}^{Q-1} \mathrm{BER}_q$, where BER_q is the output BER at the qth used subcarrier. For each Monte Carlo trial, after estimating the receiver weights on the basis of the given data record of length K, an independent record of $K_{\rm aber} = 5000$ OFDM symbols is considered to evaluate the ABER at the output of the considered receivers. All the results have been obtained by carrying out 1000 independent trials, with each run using a different set of symbols, channel parameters and noise samples.

Example 1 – ABER and ASINR versus SNR: In this example, we have studied the equalization performance of the considered receivers, as a function of the SNR. The SIR has been kept constant to 10 dB, and the sample size has been set equal to $K = 500$ symbols. Let us first consider the ABER performances of the considered receivers, which are reported in Fig. 3. It can be observed that the ideal version of the proposed CMMOE equalizer performs better than the "WPTEQ (ideal)" receiver and, moreover, it significantly outperforms the "NSL (ideal)" receiver, as well as that of the "ZF (ideal)" receiver, exhibiting only a slight performance degradation with respect to the "MMOE (ideal)" receiver. In particular, it is interesting to observe that, according to the analysis carried out in Subsection IV-A, the "CMMOE (ideal)" equalizer exhibits almost the same performance of the "MMOE (ideal)" one, for all the considered SNR values. Furthermore, it is worth noting that, as evidenced in Subsection IV-D, the unsatisfactory

[10]The performance of the MMOE receiver can be considered representative of all the different implementations of the MMSE receiver (9), such as the MMSE versions of [12], [13], [14] and the extension of [15] to hybrid CP/VC-based systems; indeed, results of computer simulations have shown that the MMOE and MMSE equalizers exhibit the same ABER performances, not only in the ideal case, but also (approximately) when they are directly estimated from the received data.

[11]The receiver of [6] has not been implemented since it is only targeted at pure CP-based systems.

[12]It should be observed that, although the receiver of [9] can be estimated from the received data either in batch mode or adaptively, unlike the proposed CMMOE equalizer, it does not allow one to perform NBI-resistant channel estimation.

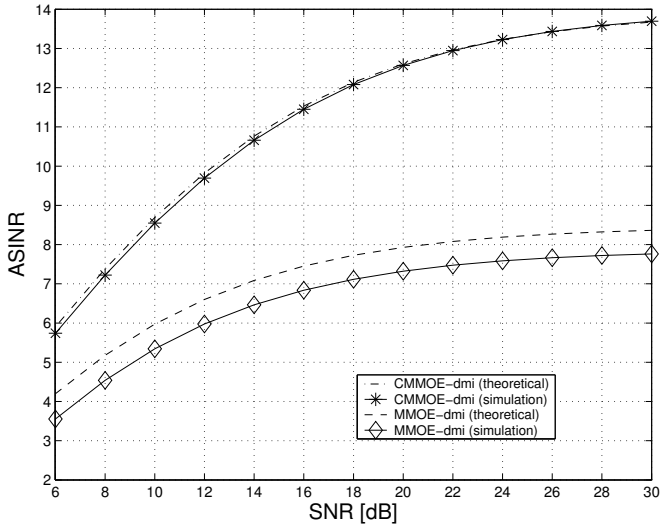

Fig. 4. ASINR versus SNR (SIR $= 10$ dB, $K = 500$ symbols).

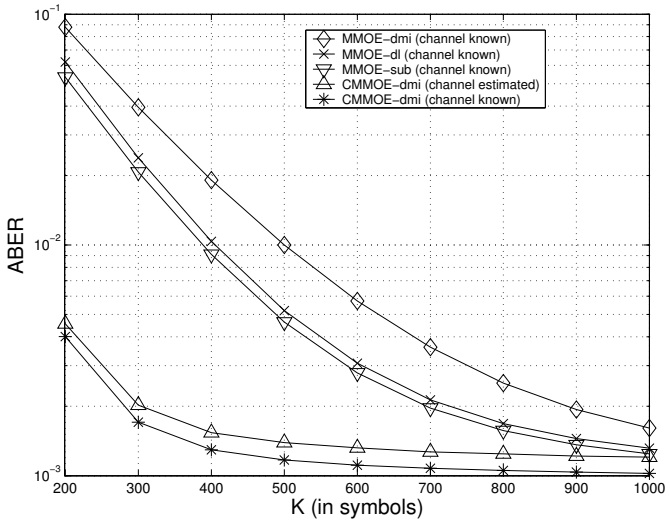

Fig. 5. ABER versus K (SNR $= 24$ dB, SIR $= 10$ dB).

performance of the NSL equalizer is basically due to the fact that the spectral position of the NBI is not located close to the VCs. As regards to the comparison between the data-estimated versions of the CMMOE and MMOE equalizers, it can be observed that the "CMMOE-dmi (channel known)" exhibits only a slight performance degradation with respect to its ideal counterpart, whereas the "MMOE-dmi (channel known)" receiver pays a significant performance penalty with respect to its ideal counterpart. Moreover, although the "MMOE-dl (channel known)" and the "MMOE-sub (channel known)" equalizers allow one to improve upon the performance of the "MMOE-dmi (channel known)" receiver, their performances are not comparable to those of the "CMMOE-dmi (channel known)" equalizer. Remarkably, the ABER curve of the "CMMOE-dmi (channel estimated)" equalizer strictly follows those of the "CMMOE-dmi (channel known)" and "WPTEQ (ideal)", for all the considered SNR values. Observe that the experimental behaviors of the data-estimated MMOE and CMMOE receivers (with channel known) are in good agreement with the results of the theoretical performance analysis carried out in Sections III and IV-B. To further corroborate this analysis, we have also reported in Fig. 4 the ASINR at the output of the "MMOE-dmi (channel known)" and "CMMOE-dmi (channel known)" equalizers; in the same plot, the simulation results (referred to as "simulation") are compared with the corresponding theoretical curves (referred to as "theoretical") [see (16) and (25)]. Results show that the theoretical expression (25) for the CMMOE equalizer agrees very well with the simulation results for all values of SNR, whereas the theoretical expression (16) for the MMOE equalizer is not as accurate as (25). Indeed, since the CMMOE equalizer provides a stronger robustness than the MMOE one against finite sample-size effects, for the considered value of the sample size K, the assumption that the predominant cause of SINR degradation in (23) is represented by $\widehat{\mathbf{r}}_{\mathbf{d}_q s_q}$ is better verified for the CMMOE receiver.

Example 2 – ABER and ASINR versus sample size K: In Fig. 5, we have reported the ABER performance only for the considered data-estimated receivers, as a function of the sample size K. The SNR and SIR have been kept constant to 24 and 10 dB, respectively. Results show that, with respect to the MMOE equalizers, the CMMOE receivers can assure a significant performance gain for a wide range of the values of the sample size K. In particular, it can be observed that, for achieving an ABER value of $2 \cdot 10^{-3}$, the "MMOE-dmi (channel known)" equalizer requires a sample size equal to $K = 900$ symbols, i.e., three times that required by the "CMMOE-dmi (channel estimated)" receiver, whereas, to achieve the same performance, the "MMOE-dl (channel known)" and "MMOE-sub (channel known)" equalizers require a sample size of about 700 symbols. Additionally, we have reported in Fig. 6 the ASINR at the output of the data-estimated DMI-based CMMOE and MMOE receivers (with channel known). Besides confirming the very good agreement between theoretical and experimental results for the CMMOE equalizer, results of Fig. 6 show that the accuracy of the theoretical expression (16) for the MMOE equalizer improves as the sample size K increases.

Example 3 – ABER versus SIR: In this example, we have studied the ABER performances of all the considered receivers, as a function of SIR. The SNR has been kept constant to 24 dB, and the sample size has been set equal to $K = 500$ OFDM symbols. It can be observed from Fig. 7 that, for all the considered SIR values, the performances of the "CMMOE-dmi (channel known)" and the "CMMOE-dmi (channel estimated)" receivers are very close to those of their ideal version, exhibiting only a slight degradation with respect to the "MMOE (ideal)" receiver. On the other hand, in comparison with the "MMOE (ideal)" equalizer, all the other data-estimated equalizers are subject to a severe performance penalty, which is almost independent of the SIR, whereas the performances of both the ZF and NSL ideal receivers strongly depend on the SIR: they start working satisfactorily only for values of SIR approaching 20 dB. Finally, note that, although the "WPTEQ (ideal)" receiver performs worse

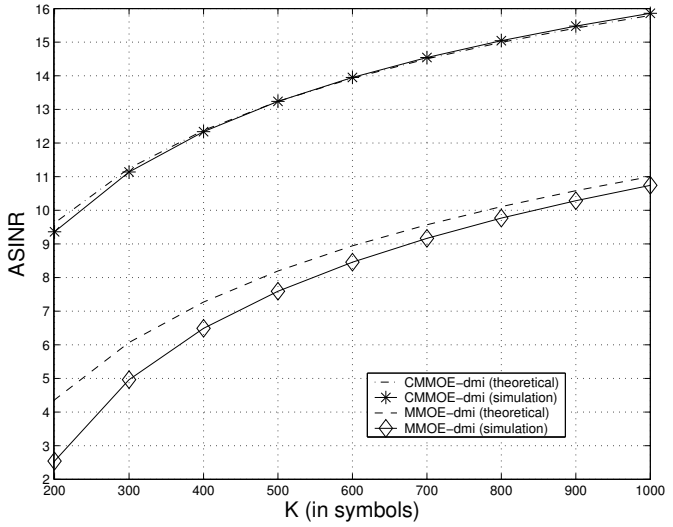

Fig. 6. ASINR versus K (SNR $= 24$ dB, SIR $= 10$ dB).

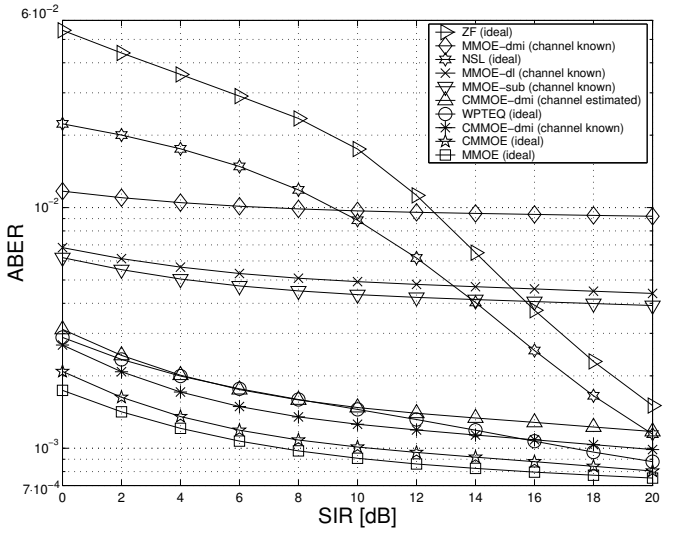

Fig. 7. ABER versus SIR (SNR $= 24$ dB, $K = 500$ symbols).

than the "CMMOE (ideal)" and "MMOE (ideal)" equalizers for all the considered SIR values, in agreement with [9], it exhibits good NBI ideal suppression capabilities and, as the SIR increases, its ABER curve approach those of the "CMMOE (ideal)" and "MMOE (ideal)" equalizers.

Example 4 – ABER versus NBI frequency-offset f_I: In this example, we have evaluated the performances of the receivers under comparison, as a function of the NBI frequency offset f_I, with SNR and SIR kept constant to 24 dB and 10 dB, respectively, and $K = 500$ symbols. More precisely, we have reported the results as a function of $\delta_I \triangleq M\,T_c\,f_I$, ranging from the midpoint of the two VCs 1 and 2 to the midpoint of the two used subcarrier 7 and 8. It is worth noting that δ_I represents the NBI frequency-offset normalized with respect to the subcarrier spacing $1/(M\,T_c)$ and, thus, when δ_I takes on an integer value, the NBI is exactly located on a subcarrier; moreover, since the NBI null-to-null bandwidth is larger than the intercarrier spacing, when f_I is located

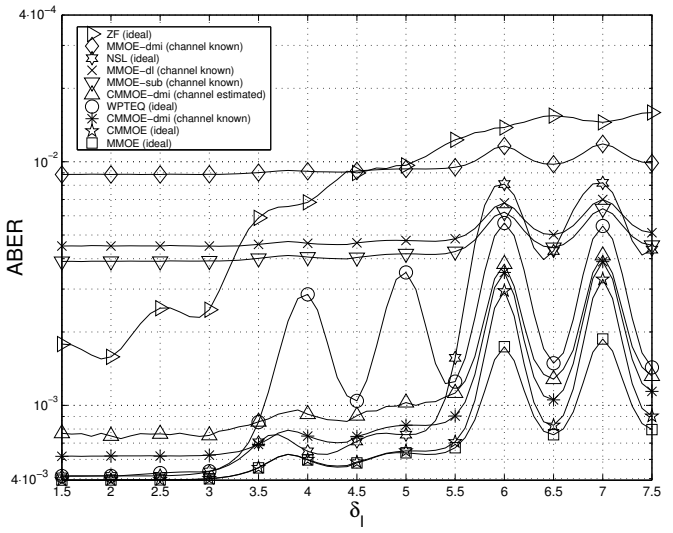

Fig. 8. ABER versus $\delta_I = M\,T_c\,f_I$ (SNR $= 24$ dB, SIR $= 10$ dB, $K = 500$ symbols).

between two subcarriers, e.g., $\delta_I = 6.5$, its main lobe overlaps with both of them. Results of Fig. 8 show that, similarly to the case of a tone interference discussed in Sections III and IV-A, the performances of both the MMOE and CMMOE receivers degrade when the NBI is located exactly on a used subcarrier; in this case, with respect to the CMMOE receivers, the corresponding MMOE receivers pay a smaller performance penalty. Furthermore, observe that the "NSL (ideal)" receiver performs comparably to the CMMOE and MMOE equalizers only when the NBI spectral position lies in proximity of the VCs. Finally, note that, except for $\delta_I \in (1.5, 3.5)$, the "WPTEQ (ideal)" equalizer performs worse than the CMMOE and MMOE ones; moreover, in comparison to the "NSL (ideal)" receiver, although it exhibits a better performance when the NBI is located in proximity of the used subcarriers, i.e., $\delta_I \in (5.5, 7.5)$, its performance rapidly degrades when the NBI spectral position moves from the VCs to the first used subcarrier.

Example 5 – ASINR versus number of iterations n for an NBI time-varying environment: In this last example, to assess the tracking performance of the proposed three-stage adaptive CMMOE equalizer when there is a drastic change in the NBI environment, we have evaluated the ASINR at the output of the RLS implementations of the CMMOE equalizer [referred to as "CMMOE-rls (channel known)"] and MMOE one [referred to as "MMOE-rls (channel known)"], as a function of the number of the iterations n, with SNR kept constant to 24 dB. In particular, we have considered the following scenario: during the first 500 iterations, the OFDM signal is corrupted by an NBI signal with $f_I = 13.5/(M\,T_c)$ and SIR $= 10$ dB; at iteration 501, the NBI vanishes, i.e., SIR $= +\infty$; at iteration 1001, the NBI reappears with the same SIR equal to 10 dB but with a different spectral placement $f_I = 17.5/(M\,T_c)$. Regarding the RLS implementation, for both the receivers under comparison we have chosen the same forgetting factor $\lambda = 0.999$ and initialization strategy with $\delta = 1$. Results

of Fig. 9 show that both the CMMOE and MMOE receivers are able to rapidly adapt themselves to this nonstationary environment, exhibiting a better tracking behavior when the NBI disappears than when it reappears.

VI. Conclusions

We have tackled the problem of synthesizing and analyzing both constrained and unconstrained maximum-SINR IBI-free equalizers for OFDM systems operating in the presence of possibly strong NBI. Specifically, the disturbance rejection capabilities of both the MMOE and CMMOE equalizers have been analyzed in depth either when the SOS of the received data are exactly known at the receiver or when they are estimated on the basis of a finite sample size, by providing easily interpretable results which show in particular that the proposed CMMOE equalizer turns out to be considerably more robust against estimation errors than the MMOE one. Furthermore, a three-stage computationally-efficient adaptive implementation of the CMMOE equalizer has been derived, wherein the IBI and NBI suppression is achieved in a fully blind mode, i.e., without requiring knowledge of the desired channel impulse response. This is the key feature that distinguishes our approach from previously proposed NBI-resistant techniques. Simulation results show that the performance of the CMMOE equalizer is sensitive not only to NBI parameters (e.g., power, bandwidth, spectral position and shape), but also to system parameters (e.g., CP length, VC number and positions).

Appendix I: Proof of Theorem 1

If the first R_{nbi} eigenvalues of $\mathbf{R}_{\boldsymbol{\jmath}\boldsymbol{\jmath}}$ are significantly different from zero, whereas the remaining ones are vanishingly small, then the EVD of $\mathbf{R}_{\boldsymbol{\jmath}\boldsymbol{\jmath}}$ can be well modeled by

$$\mathbf{R}_{\boldsymbol{\jmath}\boldsymbol{\jmath}} = \mathbf{U}_1\,\boldsymbol{\Sigma}_1\,\mathbf{U}_1^H = \underbrace{\mathbf{U}_1\,\boldsymbol{\Sigma}_1^{1/2}}_{\mathbf{J}\in\mathbb{C}^{N\times R_{\text{nbi}}}}\,\underbrace{\boldsymbol{\Sigma}_1^{1/2}\,\mathbf{U}_1^H}_{\mathbf{J}^H} = \mathbf{J}\,\mathbf{J}^H\,, \quad (34)$$

where $\boldsymbol{\Sigma}_1 \triangleq \text{diag}[\xi_1,\ldots,\xi_{R_{\text{nbi}}}] \in \mathbb{R}^{R_{\text{nbi}}\times R_{\text{nbi}}}$. Thus, let $\overline{\mathbf{C}}_q \triangleq [\sigma_s\,\overline{\mathbf{F}}_{0,q},\mathbf{J}] \in \mathbb{C}^{N\times(Q+R_{\text{nbi}}-1)}$, matrix $\mathbf{R}_{\mathbf{d}_q\mathbf{d}_q} = \sigma_s^2\,\overline{\mathbf{F}}_{0,q}\,\overline{\mathbf{F}}_{0,q}^H + \mathbf{R}_{\boldsymbol{\jmath}\boldsymbol{\jmath}} + \sigma_w^2\,\mathbf{I}_N$ can be expressed as

$$\begin{aligned}\mathbf{R}_{\mathbf{d}_q\mathbf{d}_q} &= \overline{\mathbf{C}}_q\,\overline{\mathbf{C}}_q^H + \sigma_w^2\,\mathbf{I}_N \\ &= \begin{bmatrix}\mathbf{V}_1 & \mathbf{V}_2\end{bmatrix}\begin{bmatrix}\boldsymbol{\Lambda}_1 & \mathbf{O}_{r_q\times(N-r_q)}\\ \mathbf{O}_{(N-r_q)\times r_q} & \mathbf{O}_{(N-r_q)\times(N-r_q)}\end{bmatrix}\begin{bmatrix}\mathbf{V}_1^H\\ \mathbf{V}_2^H\end{bmatrix} \\ &\quad + \sigma_w^2\,\mathbf{I}_N\,, \quad (35)\end{aligned}$$

where the diagonal matrix $\boldsymbol{\Lambda}_1 \in \mathbb{R}^{r_q\times r_q}$ collect all the nonnull eigenvalues of $\overline{\mathbf{C}}_q\,\overline{\mathbf{C}}_q^H$, with $r_q \triangleq \text{rank}(\overline{\mathbf{C}}_q) \le \min\{N, Q+R_{\text{nbi}}-1\}$, whose corresponding eigenvectors are the columns of $\mathbf{V}_1 \in \mathbb{C}^{N\times r_q}$, whereas the columns of $\mathbf{V}_2 \in \mathbb{C}^{N\times(N-r_q)}$ are the eigenvectors corresponding to the zero eigenvalues of $\overline{\mathbf{C}}_q\,\overline{\mathbf{C}}_q^H$. Reasoning as in [33], we can express $\text{SINR}_{q,\text{opt}}$ explicitly in terms of σ_w^2 as follows

$$\begin{aligned}\text{SINR}_{q,\text{opt}} &= \sigma_s^2\,\mathbf{f}_{0,q}^H\,\mathbf{R}_{\mathbf{d}_q\mathbf{d}_q}^{-1}\,\mathbf{f}_{0,q} = \frac{\sigma_s^2}{\sigma_w^2}\,\mathbf{f}_{0,q}^H\,\mathbf{V}_2\,\mathbf{V}_2^H\,\mathbf{f}_{0,q} \\ &\quad + \sigma_s^2\,\mathbf{f}_{0,q}^H\,\mathbf{V}_1\,\boldsymbol{\Lambda}_1^{-1}\mathbf{V}_1^H\,\mathbf{f}_{0,q} + O(\sigma_w^2)\,, \quad (36)\end{aligned}$$

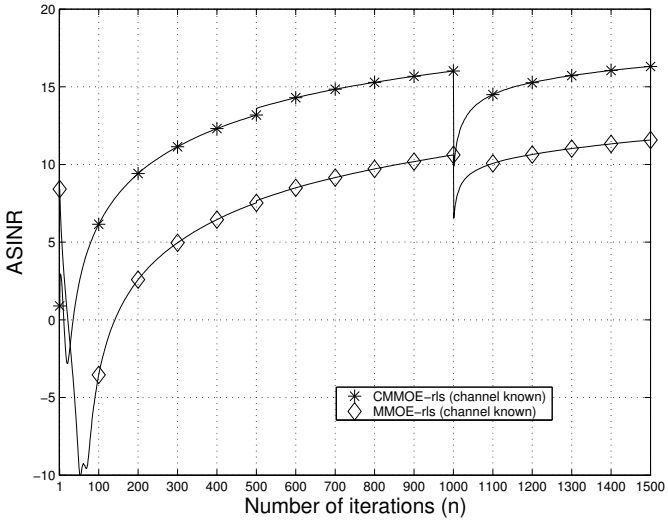

Fig. 9. ASINR versus number of iterations n (SNR = 24 dB, SIR = 10 dB, NBI time-varying environment).

which shows that, as $\sigma_w^2 \to 0$, $\text{SINR}_{q,\text{opt}} \to +\infty$, iff $\mathbf{f}_{0,q}^H\,\mathbf{V}_2\,\mathbf{V}_2^H\,\mathbf{f}_{0,q} \neq 0$, which requires that $\mathbf{f}_{0,q} \notin \mathcal{N}(\mathbf{V}_2^H) \equiv \mathcal{R}(\overline{\mathbf{C}}_q)$. This condition holds, for each q, iff $\mathbf{C} \triangleq [\sigma_s\,\mathbf{F}_0,\mathbf{J}] \in \mathbb{C}^{N\times(Q+R_{\text{nbi}})}$ is full-column rank, i.e., $\text{rank}(\mathbf{C}) = Q+R_{\text{nbi}}$, which necessarily requires that $\mathbf{C}$ is a tall matrix, i.e., condition (c1) must be satisfied. Since $\mathbf{J}$ is full-column rank by construction, condition $\text{rank}(\mathbf{C}) = Q+R_{\text{nbi}}$ necessarily requires that matrix $\mathbf{F}_0 \in \mathbb{C}^{N\times Q}$ is full-column rank, i.e., $\text{rank}(\mathbf{F}_0) = Q$. Observe that, if (c1) holds, matrix $\mathbf{F}_0$ turns out to be tall. Reasoning as in [22], it follows that $\text{rank}(\mathbf{F}_0) = Q$ iff condition (c2) holds. Therefore, let $\mathbf{E}_0 \in \mathbb{C}^{N\times N}$ denote the orthogonal projector onto $\mathcal{R}^{\perp}(\mathbf{F}_0)$, it results [34] that $\text{rank}(\mathbf{C}) = \text{rank}(\mathbf{F}_0) + \text{rank}(\mathbf{E}_0\,\mathbf{J}) = Q + \text{rank}(\mathbf{E}_0\,\mathbf{J})$, which implies that $\text{rank}(\mathbf{C}) = Q+R_{\text{nbi}}$ iff $\text{rank}(\mathbf{E}_0\,\mathbf{J}) = R_{\text{nbi}}$, i.e., the matrix $\mathbf{E}_0\,\mathbf{J} \in \mathbb{C}^{N\times R_{\text{nbi}}}$ is full-column rank. In its turn, it can be verified [20] that $\text{rank}(\mathbf{E}_0\,\mathbf{J}) = R_{\text{nbi}}$ is fulfilled iff $\mathcal{N}(\mathbf{E}_0) \cap \mathcal{R}(\mathbf{J}) = \{\mathbf{0}_N\}$ and, finally, by observing that $\mathcal{N}(\mathbf{E}_0) = \mathcal{R}(\mathbf{F}_0)$ and $\mathcal{R}(\mathbf{J}) = \mathcal{R}(\mathbf{U}_1)$, one obtains condition (c3).

Appendix II: Parameterization of matrix $\mathbf{F}_0$

First, it is worthwhile to enlighten the structure of $\mathbf{T}_0 = \mathbf{T}_{\text{cp}}\,\mathbf{W}_{\text{IDFT}}\boldsymbol{\Theta}$. To this end, observe that, by virtue of the particular structure of the matrices $\mathbf{P}$ and $\mathbf{S}$, the matrix $\mathbf{T}_0 = [\boldsymbol{\xi}_{i_0},\boldsymbol{\xi}_{i_1},\ldots,\boldsymbol{\xi}_{i_{Q-1}}]$ is obtained from $\mathbf{T}_{\text{cp}}\,\mathbf{W}_{\text{IDFT}} = [\boldsymbol{\xi}_0,\boldsymbol{\xi}_1,\ldots,\boldsymbol{\xi}_{M-1}]$ by picking its columns $\boldsymbol{\xi}_i \in \mathbb{C}^P$ located on the used subcarrier positions, i.e., for $i \in \mathcal{I}_{\text{uc}} \triangleq \{i_0,i_1,\ldots,i_{Q-1}\} \equiv \{0,1,\ldots,M-1\} - \mathcal{I}_{\text{vc}}$. Accounting for the periodicity of the complex exponentials $z_i \triangleq e^{j\frac{2\pi}{M}i}$, it can be easily shown that the ith column of $\mathbf{T}_{\text{cp}}\,\mathbf{W}_{\text{IDFT}}$ can be expressed as $\boldsymbol{\xi}_i = M^{-1/2}\,e^{-j\frac{2\pi}{M}L_{\text{cp}}i}\,\boldsymbol{\chi}_i$, for $i \in \{0,1,\ldots,M-1\}$, where we have defined the Vandermonde vector $\boldsymbol{\chi}_i \triangleq [1,z_i,z_i^2,\ldots,z_i^{P-1}]^T \in \mathbb{C}^P$. Thus, for $q \in \{0,1,\ldots,Q-1\}$, the $(q+1)$th column $\mathbf{f}_{0,q} \in \mathbb{C}^N$ of matrix $\mathbf{F}_0$ is given by

$$\mathbf{f}_{0,q} = \mathbf{H}\,\boldsymbol{\xi}_{i_q} = M^{-1/2}\,e^{-j\frac{2\pi}{M}L_{\text{cp}}i_q}\,\mathbf{H}\,\boldsymbol{\chi}_{i_q}\,. \quad (37)$$

Interestingly, due to both the Toeplitz nature of $\mathbf{H}$ and the Vandermonde structure of $\boldsymbol{\chi}_{i_q}$, it can be readily verified that $\mathbf{H}\,\boldsymbol{\chi}_{i_q} = H(e^{j\frac{2\pi}{M}i_q})\,e^{j\frac{2\pi}{M}L_h i_q}\,\boldsymbol{\zeta}_{i_q}$, with $\boldsymbol{\zeta}_{i_q} \triangleq [1, z_{i_q}, z_{i_q}^2, \ldots, z_{i_q}^{N-1}]^T \in \mathbb{C}^N$. Consequently, the matrix $\mathbf{F}_0$ can be finally parameterized as

$$\mathbf{F}_0 = \boldsymbol{\mathcal{V}}_0\,\boldsymbol{\Lambda}_0\,\boldsymbol{\mathcal{H}}_{\text{uc}}\,, \tag{38}$$

where

$$\boldsymbol{\mathcal{V}}_0 \triangleq [\boldsymbol{\zeta}_{i_0}, \boldsymbol{\zeta}_{i_1}, \ldots, \boldsymbol{\zeta}_{i_{Q-1}}] \in \mathbb{C}^{N\times Q}\,, \tag{39}$$

$$\boldsymbol{\Lambda}_0 \triangleq \frac{1}{\sqrt{M}}\,\text{diag}[e^{-j\frac{2\pi}{M}(L_{\text{cp}}-L_h)i_0}, e^{-j\frac{2\pi}{M}(L_{\text{cp}}-L_h)i_1}, \ldots, e^{-j\frac{2\pi}{M}(L_{\text{cp}}-L_h)i_{Q-1}}] \in \mathbb{C}^{Q\times Q}, \tag{40}$$

and

$$\boldsymbol{\mathcal{H}}_{\text{uc}} \triangleq \text{diag}[H(e^{j\frac{2\pi}{M}i_0}), H(e^{j\frac{2\pi}{M}i_1}), \ldots, H(e^{j\frac{2\pi}{M}i_{Q-1}})] \in \mathbb{C}^{Q\times Q}\,. \tag{41}$$

APPENDIX III: PROOF OF THEOREM 2

Since $\text{SINR}_{q,\text{opt}} \geq \text{SINR}_{q,\text{cmmoe}} = \sigma_s^2/\mathcal{P}_{q,\text{cmmoe}}$, it results that, if $\lim_{\sigma_w^2\to 0}\mathcal{P}_{q,\text{cmmoe}} = 0$, then $\lim_{\sigma_w^2\to 0}\text{SINR}_{q,\text{opt}} = +\infty$ which, according to Theorem 1, implies that conditions (c1), (c2) and (c3) are fulfilled. Let us now assume that conditions (c1), (c2) and (c3) hold. Accounting for (34) and resorting to the limit formula for the Moore-Penrose inverse [20], one has

$$\begin{aligned}\lim_{\sigma_w^2\to 0}\mathcal{P}_{q,\text{cmmoe}} &= (\mathbf{g}_{q,\text{cmmoe}}^{(\text{f})})^H\,\mathbf{J}\,\mathbf{J}^H\,\mathbf{g}_{q,\text{cmmoe}}^{(\text{f})} \\ &\quad - (\mathbf{g}_{q,\text{cmmoe}}^{(\text{f})})^H\,\mathbf{J}\,(\boldsymbol{\Pi}_0\,\mathbf{J})^\dagger\,\boldsymbol{\Pi}_0\,\mathbf{J}\,\mathbf{J}^H\,\mathbf{g}_{q,\text{cmmoe}}^{(\text{f})} \\ &= \boldsymbol{\jmath}_q^{\,T}(\mathbf{F}_0^\dagger\,\mathbf{J})\,\mathbf{P}_{\mathcal{N}(\boldsymbol{\Pi}_0\,\mathbf{J})}\,(\mathbf{F}_0^\dagger\,\mathbf{J})^H\boldsymbol{\jmath}_q\,,\end{aligned} \tag{42}$$

where $\mathbf{P}_{\mathcal{N}(\boldsymbol{\Pi}_0\,\mathbf{J})} \triangleq \mathbf{I}_{R_{\text{nbi}}} - (\boldsymbol{\Pi}_0\,\mathbf{J})^\dagger\,(\boldsymbol{\Pi}_0\,\mathbf{J}) \in \mathbb{C}^{R_{\text{nbi}}\times R_{\text{nbi}}}$ is the orthogonal projector on the subspace $\mathcal{N}(\boldsymbol{\Pi}_0\,\mathbf{J})$. Let us now characterize $\mathcal{N}(\boldsymbol{\Pi}_0\,\mathbf{J})$. Under condition (c1), the matrix $\boldsymbol{\Pi}_0\,\mathbf{J} \in \mathbb{C}^{(N-Q)\times R_{\text{nbi}}}$ turns out to be tall and, thus, the dimension of its null space is equal to the number R_{nbi} of columns minus $\text{rank}(\boldsymbol{\Pi}_0\,\mathbf{J})$. On the other hand, if condition (c2) holds, then $\mathcal{R}(\mathbf{F}_0) = \mathcal{N}(\boldsymbol{\Pi}_0)$ which, together with condition (c3), implies that $\mathcal{N}(\boldsymbol{\Pi}_0)\cap\mathcal{R}(\mathbf{U}_1) = \{\mathbf{0}_N\}$. Since $\mathcal{R}(\mathbf{U}_1) = \mathcal{R}(\mathbf{J}) = R_{\text{nbi}}$, this last relation is equivalent [20] to $\text{rank}(\boldsymbol{\Pi}_0\,\mathbf{J}) = R_{\text{nbi}}$, which means that the dimension of $\mathcal{N}(\boldsymbol{\Pi}_0\,\mathbf{J})$ is zero, implying thus $\mathbf{P}_{\mathcal{N}(\boldsymbol{\Pi}_0\,\mathbf{J})} = \mathbf{O}_{R_{\text{nbi}}\times R_{\text{nbi}}}$, hence $\lim_{\sigma_w^2\to 0}\mathcal{P}_{q,\text{cmmoe}} = 0$.

REFERENCES

[1] J.A. Bingham, "Multicarrier modulation for data transmission: an idea whose time has come," *IEEE Commun. Mag.*, pp. 5–14, May 1990.

[2] Z. Wang and G. B. Giannakis, "Wireless multicarrier communications – Where Fourier meets Shannon," *IEEE Signal Processing Magazine*, vol. 17, no. 3, pp. 29–48, May 2000.

[3] P. Chow, J. Cioffi, and J. Bingham, "A practical discrete multitone transceiver loading algorithm for data transmission over spectrally shaped channels," *IEEE Trans. Commun.*, vol. 43, pp. 773-775, Feb./Mar./Apr. 1995.

[4] D. Darsena, G. Gelli, L. Paura, F. Verde, "Widely-linear equalization and blind channel identification for interference-contaminated multicarrier systems", *IEEE Trans. Signal Processing*, vol. 53, pp. 1163-1177, March 2005.

[5] S. H. Müller-Weinfurtner, "Optimum Nyquist windowing in OFDM receivers," *IEEE Trans. Commun.*, vol. 49, pp. 417–420, March 2002.

[6] A. J. Redfern, "Receiver window design for multicarrier communication systems," *IEEE J. Select. Areas Commun.*, vol. 20, pp. 1029–1036, June 2002.

[7] D. Darsena, G. Gelli, L. Paura, and F. Verde, "Joint equalisation and interference suppression in OFDM systems," *Electronics Letters*, vol. 39, pp. 873–874, May 2003.

[8] K. Van Acker, G. Leus, M. Moonen, O. van de Wiel, and T. Pollet, "Per tone equalization for DMT-based systems," *IEEE Trans. Commun.*, vol. 49, no. pp. 109–119, Jan. 2001.

[9] K. Van Acker, T. Pollet, G. Leus, and M. Moonen, "Combination of per tone equalization and windowing in DMT-receivers," *Signal Processing*, vol. 81, pp. 1571–1579, Aug. 2001.

[10] K. Vanbleu, M. Moonen, and G. Leus, "Linear and decision-feedback per tone equalization for DMT-based transmission over IIR channels," *IEEE Trans. Signal Processing*, vol. 54, pp. 258-273, Jan. 2006.

[11] S. Trautmann and N. J. Fliege, "A new equalizer for multitone systems without guard time," *IEEE Commun. Letters*, vol. 6, pp. 34–36, Jan. 2002.

[12] S. Trautmann, T. Karp and N. J. Fliege, "Frequency-domain equalization for DMT/OFDM systems with insufficient guard interval," in *Proc. of 2002 IEEE Int. Conf. on Commun.*, New York, USA, April 2002, pp. 1646–1650.

[13] T. Karp, M. J. Wolf, S. Trautmann, and N. J. Fliege, "Zero-forcing frequency-domain equalization for DMT systems with insufficient guard interval," in *Proc. of 2003 IEEE Int. Conf. on Acoustic, Speech, and Signal Processing*, Hong Kong, China, April 2003, pp. 221–224.

[14] N. J. Fliege and S. Trautmann, "Generalized DMT/OFDM with high performance," in *Proc. of 2002 IEEE Int. Conf. on Circuits and Syst. for Commun.*, St. Petersburg, Russia, June 2002, pp. 454–459.

[15] S. Trautmann and N. J. Fliege, "Perfect equalization for DMT systems without guard interval," *IEEE J. Select. Areas Commun.*, vol. 20, pp. 987–996, June 2002.

[16] R. Nilsson, F. Sjöberg, and J. P. LeBlanc, "A rank-reduced LMMSE canceller for narrowband interference suppression in OFDM-based systems," *IEEE Trans. Communications*, vol. 51, no. 12, pp. 2126–2140, Dec. 2003.

[17] D. Darsena, G. Gelli, L. Paura, F. Verde, "NBI-resistant zero-forcing equalizers for OFDM systems", *IEEE Commun. Letters*, vol. 53, pp. 744-746, Aug. 2005.

[18] M. Honig, U. Madhow, and S. Verdù, "Blind adaptive multiuser detection," *IEEE Trans. Inform. Theory*, vol. 41, pp. 944–960, July 1995.

[19] M. Morelli and U. Mengali, "A comparison of pilot-aided channel estimation methods for OFDM systems," *IEEE Trans. Signal Processing*, vol. 49, pp. 3065–3073, Dec. 2001.

[20] A. Ben-Israel and T. N. E. Greville, *Generalized Inverses*, Springer-Verlag.

[21] R. A. Horn and C. R. Johnson, *Matrix analysis*, Cambridge University Press.

[22] A. Scaglione, G. B. Giannakis and S. Barbarossa, "Redundant filterbank precoders and equalizers Part I & II," *IEEE Trans. Signal Processing*, vol. 47, pp. 1988–2022, July 1999.

[23] J. G. Proakis. *Digital communications (2nd ed.).* McGraw-Hill, New York, 1989.

[24] H.L. Van Trees, *Optmimum Array Processing*. New York: John Wiley & Sons, 2002.

[25] D. Slepian, "Prolate spheroidal wave functions, Fourier analysis, and uncertaintly – V: the discrete case," *Bell Syst. Tech. J.*, vol. 47, pp. 1371–1430, May 1978.

[26] R.T. Behrens and L.L. Scharf, "Signal processing applications of oblique projection operators," *IEEE Trans. Signal Processing*, vol. 42, pp. 1413–1424, June 1994.

[27] L.B. Milstein, "Interference rejection techniques in spread spectrum communications," *Proc. of IEEE*, vol. 76, pp. 657–671, June 1988.

[28] M. Wax and Y. Anu, "Performance analysis of the minimum variance beamformer," *IEEE Trans. Signal Processing*, pp. 928–937, April 1996.

[29] X. Wang and H. V. Poor, "Blind multiuser detection: a subspace approach," *IEEE Trans. Inform. Theory*, vol. 44, pp. 677–690, Mar. 1998.

[30] S. Haykin, *Adaptive Filter Theory*. New York: Prentice Hall, 1996.

[31] ETSI Normalization Committee, "Channel models for HIPERLAN/2 in different indoor scenarios", Norme ETSI, available on `http://www.etsi.org`.

[32] S.M. Kay, *Fundamentals of Statistical Signal Processing: Estimation theory*. New Jersey: Prentice Hall, 1993.

[33] M.K. Tsatsanis and Z.D. Xu, "Performance analysis of minimum variance CDMA receivers," *IEEE Trans. Signal Processing*, vol. 46, pp. 3014–3022, Nov. 1998.
[34] G. Marsaglia and G.P.H. Styan, "Equalities and inequalities for ranks of matrices," *Linear and Multilinear Algebra*, pp. 269–292, Feb. 1974.

Donatella Darsena (M'06) was born in Napoli, Italy, on December 11, 1975. She received the Dr. Eng. degree *summa cum laude* in telecommunications engineering in 2001, and the Ph.D. degree in electronic and telecommunications engineering in 2005, both from the University of Napoli Federico II.

Since 2005, he has been an Assistant Professor with the Department for Technologies, University of Napoli Parthenope. Her research activities lie in the area of statistical signal processing, digital communications, and communication systems. In particular, her current interests are focused on equalization, channel identification and narrowband-interference suppression for multicarrier systems.

Giacinto Gelli was born in Napoli, Italy, on July 29, 1964. He received the Dr. Eng. degree *summa cum laude* in electronic engineering in 1990, and the Ph.D. degree in computer science and electronic engineering in 1994, both from the University of Napoli Federico II, Italy.

From 1994 to 1998, he was an Assistant Professor with the Department of Information Engineering, Second University of Napoli. Since 1998 he has been with the Department of Electronic and Telecommunication Engineering, University of Napoli Federico II, first as an Associate Professor, and since November 2006 as a Full Professor of Telecommunications. He also held teaching positions at the University Parthenope of Napoli. His research interests are in the fields of statistical signal processing, array processing, image processing, and mobile communications, with current emphasis on code-division multiple-access systems and multicarrier modulation.

Luigi Paura was born in Napoli, Italy, on February 20, 1950. He received the Dr. Eng. degree *summa cum laude* in electronic engineering in 1974 from the University of Napoli Federico II.

From 1979 to 1984 he was with the Department of Electronic and Telecommunication Engineering, University of Napoli, Italy, first as an Assistant Professor and then as an Associate Professor. Since 1994, he has been a Full Professor of Telecommunications: first, with the Department of Mathematics, University of Lecce, Italy; then, with the Department of Information Engineering, Second University of Napoli; and, finally, from 1998 he has been with the Department of Electronic and Telecommunication Engineering, University of Napoli Federico II. He also held teaching positions at the University of Salerno, Italy, at the University of Sannio, Italy, and the University Parthenope, Napoli, Italy. In 1985-86 and 1991 he was a Visiting Researcher at the Signal and Image Processing Laboratory, University of California, Davis. At the present time, his research activities are mainly concerned with statistical signal processing, digital communication systems and medium access control in wireless networks.

Francesco Verde was born in Santa Maria Capua Vetere, Italy, on June 12, 1974. He received the Dr. Eng. degree *summa cum laude* in electronic engineering in 1998 from the Second University of Napoli, and the Ph.D. degree in information engineering in 2002, from the University of Napoli Federico II.

Since 2002, he has been an Assistant Professor with the Department of Electronic and Telecommunication Engineering, University of Napoli Federico II. His research activities lie in the area of statistical signal processing, digital communications, and communication systems. In particular, his current interests are focused on cyclostationarity-based techniques for blind identification, equalization and interference suppression for narrowband modulation systems, code-division multiple-access systems and multicarrier modulation systems.